Pre-normative REsearch for Safe use of Liquid Hydrogen (PRESLHY)

Fuel Cells and Hydrogen Joint Undertaking (FCH 2 JU)

Grant Agreement Number 779613

Summary of experiment series E5.2 (Combustion tube) results

Deliverable Number:	5.5 (D21)
Version	4.0
Author(s):	A. Veser, ProScience A. Friedrich, ProScience G. Necker, ProScience A. Denkevits, KIT M. Kuznetsov, KIT T. Jordan, KIT
Submitted Date:	18 March 2021
Due Date:	30 November 2018
Report Classification:	Confidential

History		
Nr.	Date	Changes/Author
1.0	5.7.2019	Original version by A. Friedrich, A. Veser and T. Jordan (PS/KIT)
2.0	9.9.2020	Description of experimental set-up by A Denkevits and G. Necker (KIT/PS)
3.0	10.10.2020	Data processing by M. Kuznetsov and A. Denkevits (KIT)
4.0	18.03.2021	Data processing by M. Kuznetsov and A. Denkevits (KIT)

Review			
Version	Name	Organisation	Date
1.0	Simon Jallais	AirLiquide	24.03.2021
2.0	Dmitriy Makarov	UU	15.04.2021
3.0	Jennifer Wen	WU	16.04.2021

Approvals			
Version	Name	Organisation	Date

Acknowledgements, Preface and Disclaimer

The PRESLHY project has received funding from the Fuel Cells and Hydrogen 2 Joint Undertaking under the European Union's Horizon 2020 research and innovation programme under grant agreement No 779613.

This report contain the "meta data" of the respective experiments, providing detailed description of the experimental set-up, sensors and result data storage. The actual result data will be provided via KITopen. Also detailed evaluation of the results, e.g. determining the combustion limits, as well as any modelling work is excluded here and left for subsequent work.

Because of the interrelation with the published result data it is intended to turn this confidential report into a public one.

Publishable Short Summary

In the frame of the PRESLHY project more than 100 experiments on hydrogen – air flame propagation regimes in a shock tube at cryogenic temperatures were conducted with the combustion tube at the KIT HYKA test site. More than half of the experiments were carried out at cryogenic temperatures (between approx. 80 K and 130 K). The rest of the tests were conducted at ambient conditions as the reference data. It was however possible to provide experimental data at various H_2 concentrations from 8 to 60 Vol. %H_2 and 3 blockage ratios (BR = 0, 0.3 and 0.6). During the course of the experiments, many experimental difficulties and peculiarities specific for cryogenic temperatures were encountered. Critical conditions for flame acceleration to the speed of sound and to the detonation onset were experimentally identified for hydrogen-air mixtures at cryo-temperatures. The critical expansion ratio and detonation cell sizes as function of temperature were experimentally measured for hydrogen-air mixtures. It was also found that the danger of hydrogen combustion and explosion in terms of maximum combustion pressure is 2-3 times higher than at ambient temperatures because of several times higher density of the combusted substance. Then, even for sonic deflagration at cryogenic temperatures, the maximum pressure might be higher than the detonation pressure at ambient conditions. The data obtained in current work can be used for safety distance assessment for LH2 safety applications.

Key words

Hydrogen, Liquid hydrogen (LH2), Cryogenic temperatures, Flame acceleration, Detonation onset, Detonation cell size, Combustion pressure

Abbreviations

LH2	Liquid Hydrogen
LOX	Liquid Oxygen
LN2	Liquid Nitrogen
BR	Blockage Ratio
LFL	Lower Flammability Limit
UFL	Upper Flammability Limit
FA	Flame Acceleration
DDT	Deflagration – to – Detonation Transition

Table of Contents

Acknowledgements, Preface and Disclaimer iii
Publishable Short Summary iv
Key words iv
Abbreviations iv
List of figures 1
1 Purpose of the Tests – Knowledge Gap Addressed 4
2 General Description of the Experimental Set-up 4
3 Combustion Tube Test Procedure 10
4 Instrumentation of the Combustion Tube-facility 10
4.1 Estimate of Measurement Errors 13
5 Experimental results. Warm tests 14
6 Experimental results. Cryogenic tests 24
7 Discussion 43
8 Data acquisition and data archiving. 47
9 Summary, Conclusions and Outlook 50
10 References 51

List of figures

Figure 1. Shock Tube with supporting structure. 4

Figure 2. Shock Tube without (left) and with (right) the LN2 basin. 5

Figure 3. Front flange (left) and end flange. 5

Figure 4. Port locations. 6

Figure 5. Clockwise: Front flange with ignition device, end flange, photo diode assembly, low pressure sensor. 8

Figure 6. Ignition device. 9

Figure 7. Obstacles grid. 9

Figure 8. Gas filling system. 9

Figure 9. Light gauge adaptor. 11

Figure 10. A comparison of light signal (pink line) and pressure record (red line) for different compositions (vol. H_2): (a) 10.4%; (b) 11.3%; (c) 9.2%; (d) 8.1%. 12

Figure 11. Distance-time diagram for subsonic deflagration of 45% vol. H_2 mixture: flame trajectory (blue dotted line); light signal (blue solid line); pressure signal (red and pink solid lines). 15

Figure 12. Distance-time diagram for sonic deflagration and detonation transition of 30% vol. H_2 mixture: flame trajectory (blue dotted line); shock wave trajectory (green line); light signal (blue solid line); pressure signal (red and pink solid lines). The star corresponds to DDT point. 15

Figure 13. Characteristic velocity in Mach numbers (left) and combustion pressure (right) as function of expansion ratio for hydrogen-air and hydrogen-oxygen-nitrogen mixtures 18

Figure 14. Calculations for run-up-distances X_D for rough/smooth and obstructed tubes. 18

Figure 15. Characteristic pressure (left) and flame velocity (right) as function of expansion ratio at ambient conditions: black dashed line is a cut-off line at $\sigma^*=3.75$. 21

Figure 16. Experimental characteristic pressure (left) and flame velocity (right) as function of expansion ratio in obstructed tube (BR=60%) at ambient conditions. 22

Figure 17. Experimental characteristic pressure (left) and flame velocity (right) as function of hydrogen concentration in smooth tube (BR=0%) at cryogenic and ambient temperature: experimental data (open points); theoretical calculations (dotted lines). 25

Figure 18. Comparison of flame velocity in smooth tube (BR=0%) at cryogenic and ambient temperatures: c_p is the speed of sound in combustion products; 20% vol. H_2-air (left); 50% vol. H_2-air (right). 27

Figure 19. Comparison of flame velocity for detonation regimes in smooth tube (BR=0%) at cryogenic and ambient temperatures: c_p is the speed of sound in combustion products; 29% vol. H_2-air (left); 45% vol. H_2-air (right). 27

Figure 20. Distance-time diagram for sonic deflagration of 16.1% vol. H_2 at 102.7 K: flame trajectory (blue dotted line); light signal (pink solid line); pressure signal (red and green solid lines); shock wave trajectory (green dashed line) 29

Figure 21. Distance-time diagram for sonic deflagration of 19.9% vol. H_2 at 99.6 K: flame trajectory (blue dotted line); light signal (pink solid line); pressure signal (red and green solid lines); shock wave trajectory (green dashed line). 29

Figure 22. Distance-time diagram for detonation transition in 45% vol. H_2 (T=106 K): flame trajectory (blue dotted line); shock wave trajectory (red and green dashed lines); light signal (pink solid line); pressure signal (red and green solid lines); the star is DDT point. 30

Figure 23. Distance-time diagram for sonic deflagration of 50% vol. H_2 at 102 K: flame trajectory (blue dotted line); light signal (pink solid line); pressure signal (red and green solid lines); shock wave trajectory (green dashed line) 30

Figure 24. Experimental characteristic pressure (left) and flame velocity (right) as function of expansion ratio in obstructed tube (BR=30%) at cryogenic temperature (T=102.6K): black dashed line is a cut-off line at σ^*=12.5. 33

Figure 25. Experimental combustion pressure (left) and flame velocity (right) as function of hydrogen concentration in obstructed tube (BR=30%) at cryogenic and ambient temperature: experimental data (open points); theoretical calculations (dotted lines). 33

Figure 26. Distance-time diagram for slow deflagration of 15.2% vol. H_2 at 109.3 K: flame trajectory (blue dotted line); light signal (pink solid line); pressure signal (red and green solid lines); shock wave trajectory (green dashed line). 35

Figure 27. Distance-time diagram for sonic deflagration of 17.8% H_2 at 106.9 K: flame trajectory (blue dotted line); light signal (pink solid line); pressure signal (red and green solid lines). 35

Figure 28. Distance-time diagram for sonic deflagration of 22.3% vol. H_2 at 108.6 K: flame trajectory (blue dotted line); light signal (pink solid line); pressure signal (red and green solid lines); shock wave trajectory (green dashed line). 36

Figure 29. Distance-time diagram for quasi-detonation in 28.3% vol. H_2 (T=111.8 K): flame trajectory (blue dotted line); shock wave trajectory (green dashed lines); light signal (pink solid line); pressure signal (red and green solid lines). 36

Figure 30. Critical expansion ratio as function of initial temperature based on experiments in obstructed tube (BR=30%). 37

Figure 31. Experimental characteristic pressure (left) and flame velocity (right) as function of expansion ratio in obstructed tube (BR=60%) at ambient conditions: black dashed line is a cut-off line at σ^*=12.5. 38

Figure 32. Comparison of experimental combustion pressure (left) and flame velocity (right) in obstructed tube (BR=60%) at cryogenic and ambient temperature: experimental data (open points); theoretical calculations only for cryogenic temperatures (dotted lines). 39

Figure 33. Critical expansion ratio as function of initial temperature based on experiments in obstructed tube (BR=60%). 41

Figure 34. Distance-time diagram for slow deflagration of 12.5% vol. H_2 at 94.5 K: flame trajectory (blue dotted line); light signal (pink solid line); pressure signal (red and green solid lines). 42

Figure 35. Distance-time diagram for sonic deflagration of 45% vol. H_2 at 94.1 K: flame trajectory (blue dotted line); light signal (pink solid line); pressure signal (red and green solid lines). 42

Figure 36. Dynamic pressure as a function of flow velocity calculated for stoichiometric hydrogen-air mixture at two temperatures. 43

Figure 37. Maximum combustion pressure as function of characteristic flame velocity for the experiments in a smooth tube (BR=0%). 44

Figure 38. Maximum combustion pressure as function of characteristic flame velocity for the experiments in obstructed tube (BR=30%). 44

Figure 39. Maximum combustion pressure as function of characteristic flame velocity for the experiments in obstructed tube (BR=60%). 44

Figure 40. Theoretical maximum combustion pressure as function of hydrogen concentration at different initial temperatures. 45

Figure 41. Critical expansion ratio as function of initial temperature based on experiments in obstructed tubes (BR=30% and BR = 60%). 45

Figure 42. Experimental detonation cell size at cryogenic temperature T=100 K in comparison with the data at ambient temperature T = 293 K. 47

Figure 43. The structure of data file: (a) header; (b) start time of each channel; (c) data. 48

Figure 44. Distance-time diagram PT0-24-long-RT. wmf for the test PT0-24 (15.2% vol. H_2, BR=0%, T=293 K). 50

1 Purpose of the Tests – Knowledge Gap Addressed

In the work package WP5.2 of the PRESLHY, the flame propagation regimes at cryogenic temperatures are investigated by the project partners Karlsruhe Institute of Technology (KIT) and Pro-Science (PS).
The objective is to evaluate the critical conditions for flame acceleration (FA) and detonation transition (DT) for gaseous hydrogen-air mixtures at cryogenic temperatures, without the presence of condensed oxygen and nitrogen. The data are required for safety analysis to evaluate the strongest possible combustion pressure and safety distances for cryogenic hydrogen explosions.

2 General Description of the Experimental Set-up

The facility was installed in a tent behind the main HyKA building. A nearby container housed the equipment for data acquisition.

The facility consists mainly of a stainless steel tube 5 m long with an outer diameter of 73 mm and an inner diameter of 54 mm. The production of this tube took more than 9 months at the main workshop of the KIT Campus North. Despite this long time, most sealing surfaces for the port required rework to remove scratches on the sealing surfaces. The drawing (Figure 1. Shock Tube with supporting structure.

) shows the tube with the support structure. Additional frames (Figure 2) above the tube provided support for the numerous cables.

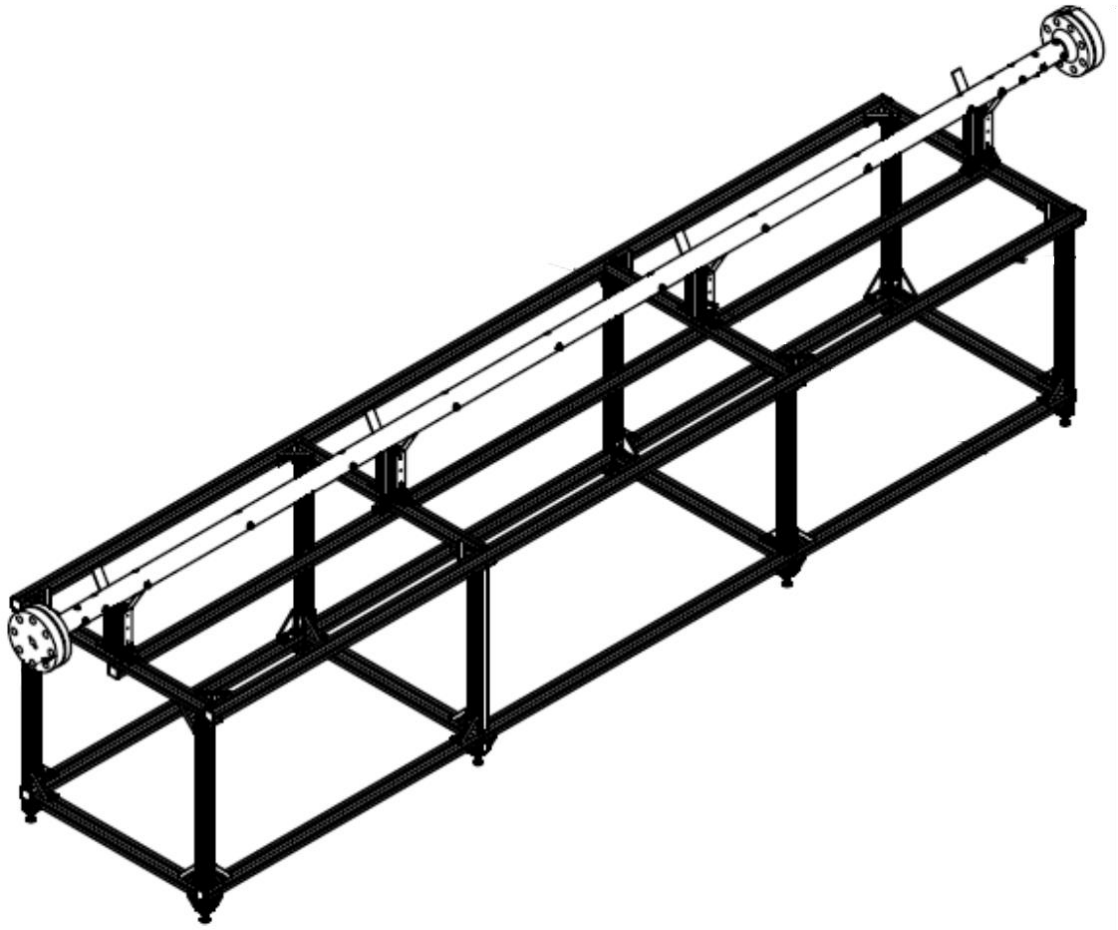

Figure 1. Shock Tube with supporting structure.

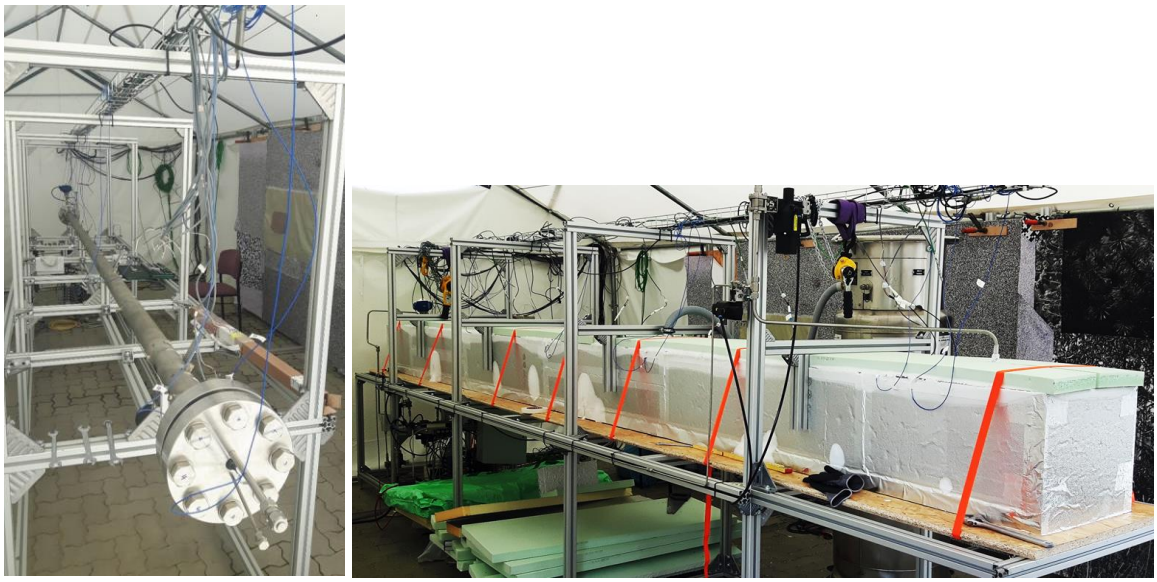

Figure 2. Shock Tube without (left) and with (right) the LN2 basin.

A basin (Figure 2, right) is fabricated of stainless steel insulated with Styrofoam provided the cooling. The basin was filled with varying amounts of liquid nitrogen LN2.

Both sides of the tube end with flanges. The flanges are sealed with PTFE coated grooved metal gaskets suited for low temperatures (73 K) and high pressures (400 bar).

The front flange (Figure 3, left) has ports for:

a. Gas inlet
b. Ignition device
c. Thermocouple (unused)

The end flange (Figure 3, right) has ports for:

a. Gas-Outlet
b. Pressure Sensor
c. Thermocouple

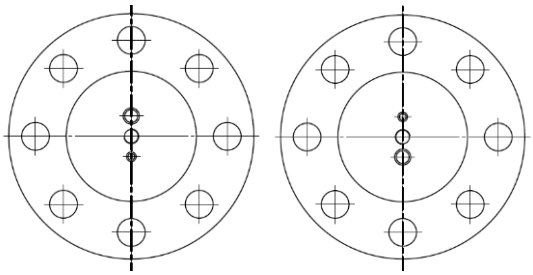

Figure 3. Front flange (left) and end flange.

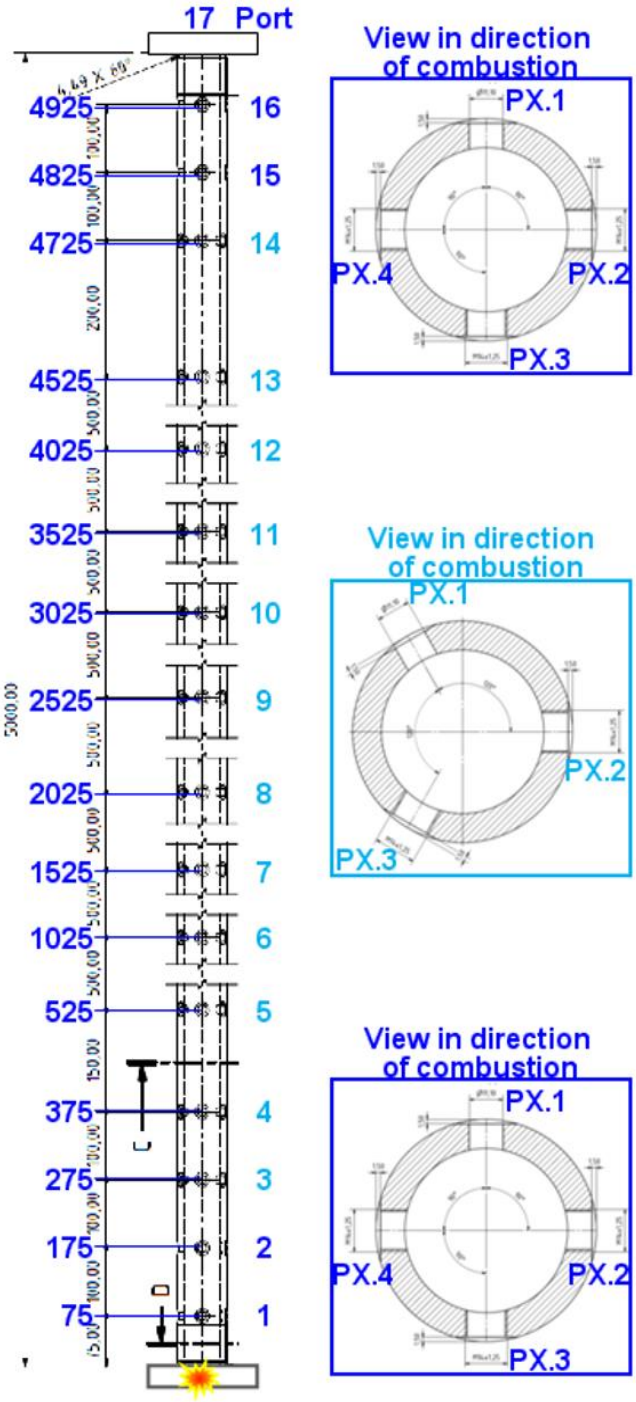

Figure 4. Port locations.

Along the tube, 52 ports in 16 cross sections (Figure 4) have been placed for pressure sensors and photodiode assemblies. The distance from the inlet port where the ignition takes place and the type of sensor is listed in Table 1. A standard automotive spark plug was used for ignition together with a matching HV generator (Bosch type). Figure 6 shows the ignition device. For some mixtures enriched with hydrogen or approaching the flammability limits a glow plug with a heating element was used. The problem, in this case, was that the mixture in the vicinity of the igniter was heated up because of the longer induction time to ignition and also the ignition moment was not exactly known as for the spark plug.

Table 1: List of sensors.

Name	Channel	Port	Distance [mm]	Sensor	Type
P01	1	2.1	175	37612	112A05
P02	2	2.2	175	6806	116B
P03	3	5.2	525	37617	112A05
P04	4	5.1	525	6807	116B
P05	5	7.1	1525	37614	112A05
P06	6	7.3	1525	6805	116B
P07	7	9.1	2525	37615	112A05
P08	8	9.2	2525	6804	116B
P09	9	11.2	3525	37600	112A05
P10	10	11.1	3525	6809	116B
P11	11	16.1	4925	37613	112A05
P12	12	16.2	4925	6811	116B
P13	13	17.0	5000	37601	112A05
F01	14	1.1	0.075	Photodiode	InGaAs
F02	15	2.4	0.175	Photodiode	InGaAs
F03	16	3.1	0.275	Photodiode	InGaAs
F04	17	4.1	0.375	Photodiode	InGaAs
F05	18	5.3	0.525	Photodiode	InGaAs
F06	19	6.1	1.025	Photodiode	InGaAs
F07	20	7.2	1.525	Photodiode	InGaAs
F08	21	8.2	2.025	Photodiode	InGaAs
F09	22	9.3	2.525	Photodiode	InGaAs
F10	23	10.1	3.025	Photodiode	InGaAs
F11	24	11.3	3.525	Photodiode	InGaAs
F12	25	12.1	4.025	Photodiode	InGaAs
F13	26	13.1	4.525	Photodiode	InGaAs
F14	27	15.1	4.825	Photodiode	InGaAs
F15	28	16.4	4. 925	Photodiode	InGaAs

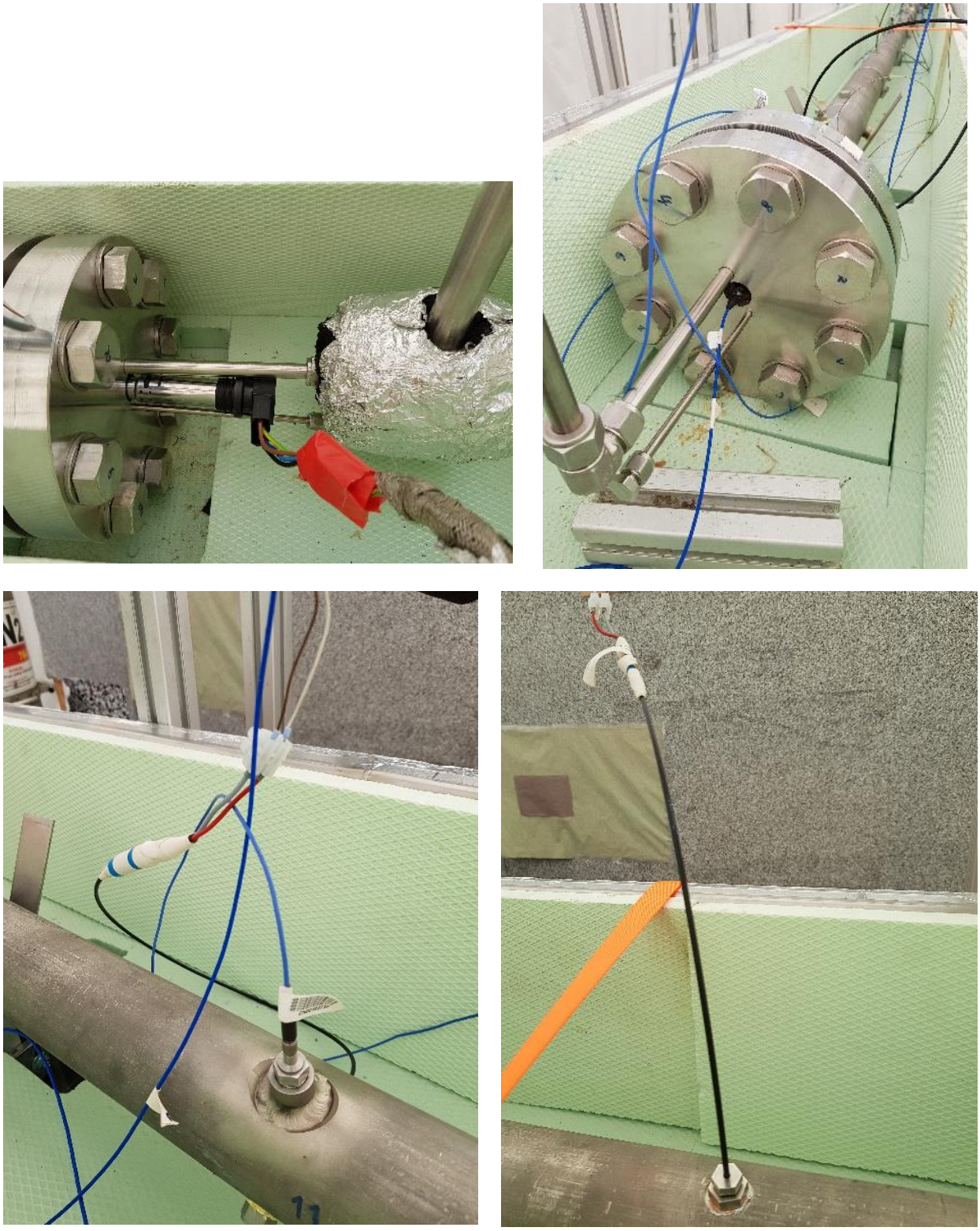

Figure 5. Clockwise: Front flange with ignition device, end flange, photo diode assembly, low pressure sensor.

The experiments on hydrogen flame propagation have been conducted in a tube geometry with 3 different blockage ratios BR = 0, 30 and 60%. Here the blockage 0% corresponds to a smooth tube without obstacles. The blockages 30 and 60% are provided by a set of metal

rings spaced by the tube diameter. Stainless steel rings of appropriate cross-sections on threaded bars lead to blockage ratios of 30 % or 60 %. The blockage ratio is defined as follows: $BR = 1 - d^2/D^2$, where d is the internal diameter of the obstacle ring; D is the inner tube diameter. Nuts fixed the distance equal to tube diameter between the rings on the bars. The obstacles (Figure 7) are 10 mm thick and their exact mid-to-mid distance was 50 mm. All ports and sensors are placed midway in between the obstacle positions.

The scheme of the setup for the gas management is shown in Figure 8.

Figure 6. Ignition device.

Figure 7. Obstacles grid.

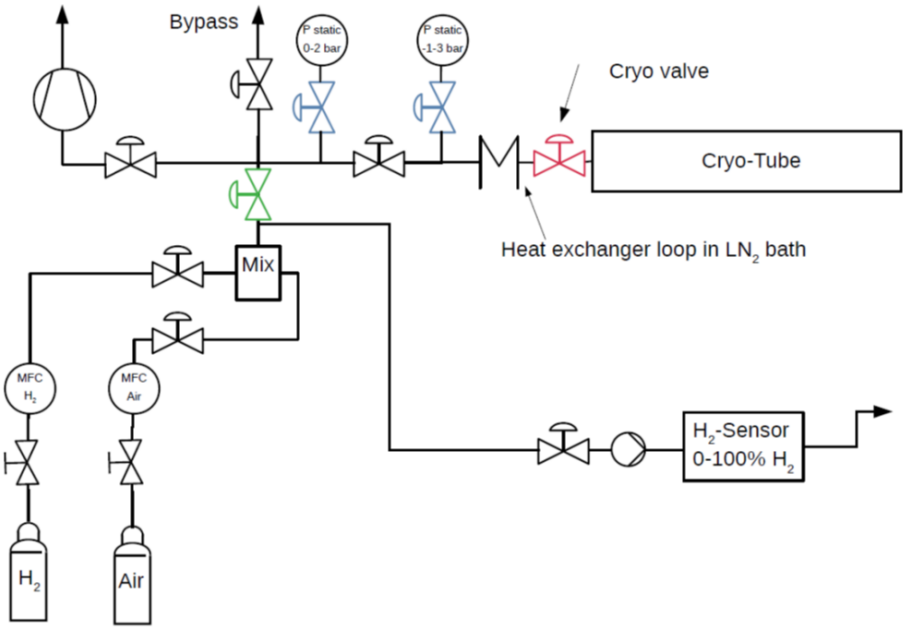

Figure 8. Gas filling system.

3 Combustion Tube Test Procedure

The experimental procedure was very different for ambient initial conditions and cryogenic temperatures. Only the "Cryo valve" is exposed to LN_2 prior to the cryogenic experiments. All other valves and devices are at ambient temperature. All valves have pneumatic actuators. The original plan was to fill the evacuated tube using 2 Mass Flow Controllers (MFC, Bronkhorst) to provide desired concentrations. It turned out, that it was impossible to fill the tube with a consistent and reproducible mixture this simple way, because the MFCs show significant oscillations of the flow rates, when used to fill a low-pressure reservoir. The oscillations were observed up to a reservoir/tube pressure of approx. 0.8 bar. There was no gas-cooling loop in the LN_2 bath, because of the possibility of LO_2 condensation at least for some concentrations. Therefore, the piping of the tube (Figure 8) was modified from the beginning and experimental procedure was adjusted as follows:

1) The tube was purged with dry compressed N_2.
2) The tube was evacuated down to < 1 mbar (limited by the vacuum pump), including all the gas lines and the mix chamber excluding the MFCs themselves. The pressure was checked with a static pressure manometer P1 (0-2) bar.
3) The bath was filled with liquid N_2. The temperature of the tube wall was controlled outside at 3 points along the tube with thermocouples clamped to the wall.
4) A preliminary mixture was prepared with 2 MFCs of H_2 and synthetic air (N_2+O_2, purchased). A H_2 sensor checked the H_2 concentration in this mixture. If necessary, the flow rates of the MFCs were adjusted. During this step the mixture was released to the air using the bypass at the inlet side.
5) When the preliminary mixture had an acceptable concentration, the valve to the tube was opened and the tube was filled. During this step the mixture flows through a pipeline loop put below LN2 level to cool mixture down before entering the tube.
6) When the pressure inside the tube was slightly above ambient pressure, the bypass valve at the outlet side was opened, the Sensor 1 valve was closed and the Sensor 2 valve was opened. The mixture was kept flowing through the tube until the concentration at the outlet side reached a stable value. If necessary, the flow rate was adjusted to achieve the desired H_2 concentration.
7) When the gas temperature inside and mixture pressure are stabilized, all the valves are closed, the tube is ready for the test.
8) Test start: the mixture is ignited triggering the data acquisition.
9) The combustion products pressure is measured by pressure transducer P02 (measured pressure range from -1 to 3 bar), their temperature evolution is registered with 2 thermocouples installed inside the tube.
10) The procedure repeats from point 2, except point 3.

The number of test repetitions is limited, because the cooled tube acts as a cold trap. It is nearly impossible to remove the condensed combustion products by pumping at temperatures below 183 K. The vacuum pump used was a Leybold SCROLLVAC SC 5.

4 Instrumentation of the Combustion Tube-facility

The small dimension and the cryogenic conditions in and around the tube imposed some limitations on the selection of sensors. Two types of dynamic pressure sensors with p_{max} = 6.9 bar (PCB 116B) and 345 bar (PCB 112A05) were used. These are special cryogenic sensors suitable for temperatures even lower than certified -100C (173K). These sensors have no built-in charge converters. Therefore, "In-Line Charge Converters" had to be used in the signal path between the sensors and the data acquisition system "PCB Sensor Signal

Conditioner Series 481". For the pressure sensor PCB 116B the converter PCB 422E2 and for the sensor PCB 112A05 the convertor PCB 422E53 were employed. The charge converters are outside the cold region. The low-pressure sensors were mounted in adaptors welded to the tube, because of their bigger size. To avoid deformation during the welding, these ports are distributed helically in the positions along the tube. The high-pressure sensors were directly screwed into the tube wall using adaptors provided by the sensor manufacturer. The adaptors for optical fibers for the photo sensors and the high-pressure sensors have the same thread. All sensors were mounted flush to the inner tube wall.

To monitor the cooling process, four thermocouples (type K) were placed at the outer tube surface, two thermocouples were inside the tube, just at the inner surface. Their distances from the front flange were 22.5 cm, 102.5 cm, 103 cm, 227 cm, 378 cm and 472.5 cm respectively. The thermocouples at 102.5 cm and 472.5 cm were inside the tube.

After some experimentation, due to the low hydrogen flame emissivity, an InGaAs photodiode was chosen as the photo sensor. A special amplifier made in the electronics workshop at KIT several years ago, biased and amplified the photo sensors. Because of the limited space availability and uncertainty about ability of the photo sensor to withstand the low temperatures the photo sensor was mounted outside the LN_2 bath and light was guided to the sensor by a polymer optical fiber (3mm O.D.). An adaptor with a quartz glass plate (6 mm dia., 3 mm thick, see position no. 32 in Figure 9) between two PTFE rings (position no. 33) provided the vacuum-tight sealing to the inner of the tube. Positions no. 30 and no. 31 in Figure 9 are the inner and outer screws of the adaptor. The diameter of the inner bore, where the light guide is placed, is just 3 mm. The other end of the light guide is fixed to the photodiode by adhesive tape.

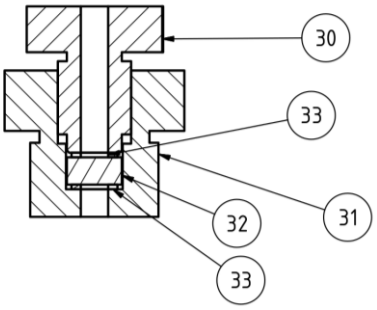

Figure 9. Light gauge adaptor.

However, the sensitivity of InGaAs photodiodes was not sufficient enough to register flames for very lean hydrogen-air mixtures in the range of hydrogen fractions from 8 to 12% vol. Then, it was decided to use thermally unprotected pressure sensors as backup thermal sensors because of the extremely high sensitivity of the piezo-cristal to the temperature. Such an unprotected pressure sensor gives a light signal as a deviation in an opposite direction compared to the pressure signal but very similar to the light signal with a negative sign, see Figure 10. The figure shows that with lower hydrogen concentration the light signal is getting weaker and becomes comparable to the noise, while the negative pressure signal remains stable and suitable for processing.

For the simultaneous data acquisition of the pressure and photo sensor signals, we used a MF Instruments/Elsys TransPC. The temperatures were measured with type K thermocouples attached to the temperature input module NI 9214 and the static pressures sensors were attached to a NI 9205 input module using a Leybold DI 2000 connector

(operating in the pressure range 0 to 2000 mbar) and a Wika S20 pressure transmitter (operating in the range of pressures -1 to 3 bar).

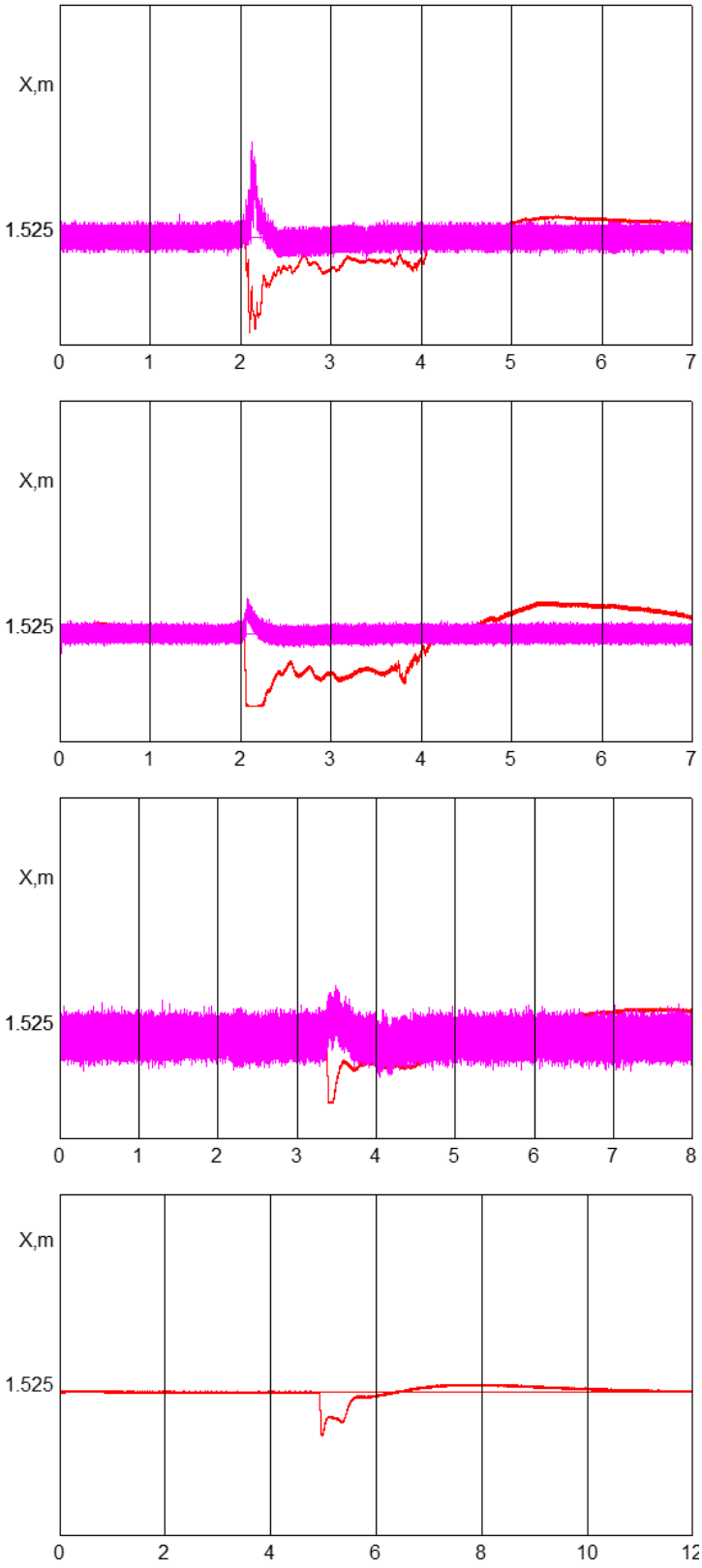

Figure 10. A comparison of light signal (pink line) and pressure record (red line) for different compositions (vol. H_2): (a) 10.4%; (b) 11.3%; (c) 9.2%; (d) 8.1%.

4.1 Estimate of Measurement Errors

The accuracy of the sensors used in the experiments is given in the table below. The values were taken from the respective manuals for ambient temperature conditions. The pressure sensors are suited for lower than the certified temperatures. For cryogenic temperatures no data is available.

Table 2. Accuracy of the sensors used in the Shock Tube experiments.

Sensor	**Manufacturer**	**Type (Range)**	**Non-linearity @ 290 K**
Static pressure	WIKA	S-20 (-1- 3 bar)	< 0.125% FS
Static pressure	Leybold	DI2000 (0-2000 mbar)	0.2 % FS
Dynamic pressure	PCB	PCB 116B + PCB 422E2	1%
Dynamic pressure	PCB	PCB 112A05 + PCB 422E53	1%
H_2-Sensor	Messkonzept	FTC300 (100% H_2)	< 1% FS
Temperature	KIT-Workshop	Type K, d = 0.36 mm	1.66 °C

In the experiments the thermocouples are exposed at cryogenic temperatures and their deviation from the temperature of LN2 (77 K) was measured in a separate test. Table 3 shows the calibration of thermocouples at the ambient temperature T_a = 17°C and cryogenic temperature T_c = 77 K provided by LN2 filled the bath where the shock tube is put in. We assume that the constant uniform temperature of 77 K in the whole tube is established.

Table 3. Calibration of thermocouples used in the Shock Tube experiments.

Thermocouples			**Temperature T, K**	
Number	**Distance, cm**	**Position**	**Ambient**	**Cryogenic**
Real			293.15	77
1	22.5	outer	293.8	98.1
2	102.5	inner	294.4	97.9
3	103	outer	295.55	98.0
4	227	outer	295.0	98.4
5	378	outer	294.4	98.1
6	472.5	inner	293.0	98.0

The table shows that the measured temperature deviates more from the LH2 temperature of 77 K. The difference reaches 21.1 degrees at 77 K. Then, a linear correlation is used to adjust the measured temperature to the real temperature. By the averaging, it leads to the linear correction with an RMS = ± 0.18 K:

$$T_r\,[K] = 1.1013 \cdot T_m\,[K] - 31.024, \quad (1)$$

where T_r and T_m are the real and measured temperatures in Kelvin. An actual initial temperature for each test was assumed to be an average for all six thermocouples.

5 Experimental results. Warm tests

The individual tests are named starting with the two letters “PT” followed by the blockage ratio (0, 30, and 60) and if the test was at low temperature, a capital “C” is appended. A hyphen and a sequence number end the name. “PT60C-50” is the test number 50 with a blockage ratio 60 % at cryogenic temperature.

A series of reference tests at ambient pressure and temperature with different tube blockages 0, 30 and 60% were conducted. Table 4 lists the tests in a smooth tube at the ambient temperature of about 293K. These tested scenario mainly involved relatively slow subsonic deflagration registered due to a longer run-up-distance (RUD) to detonation than the length of the tube itself. The only stoichiometric mixture was able to detonate at the shock wave reflection on the far end flange. Figure 11 and Figure 12 present an experiment as a sequence of signal – time histories located vertically in accordance with the position of each sensor along the tube. The horizontal axis is the time scale. The slope of the line between two characteristic peaks belonged to two different sensors gives the velocity of a certain process (flame or shock propagation). Figure 11 and Figure 12 show an example of two different flame propagation regimes: (1) subsonic deflagration, and (2) sonic deflagration followed by detonation transition. The flame (blue line) accelerates in a smooth tube very slowly. For 45% vol. H_2-mixture (Figure 11), the run-up distance to the fast sonic flame was larger than the tube length. According to paper [1], the run-up distance to detonation in a smooth channel is roughly 500 times larger than the detonation cell size $x_D = 500\ \lambda$. The calculated data on detonation cell size is given in Table 6. Thus, independent of the high mixture reactivity and small detonation cell size $\lambda = 16.8$ mm, the flame for the mixture of 45% vol. H_2 in air does not accelerate to the speed of sound and does not detonate because $x_D = 500\ \lambda = 8400$ mm is significantly larger than the available length of the tube L=5000 mm.

Table 4: Experiments in a smooth tube (blockage ratio 0%) at ambient temperature.

Name	H_2, vol %	Temperature [K]	Regime
PT0-01	14.8	293	S
PT0-02	19.5	293	S
PT0-03	19.6	293	S
PT0-04	19.6	293	S
PT0-05	28.4	293	F/D
PT0-06	28.2	293	F/D
PT0-24	15.2	293	S
PT0-25	15	293	S
PT0-26	12.35	293	S
PT0-27	11.3	293	S
PT0-28	10.4	293	S
PT0-29	9.2	293	S
PT0-30	8.1	293	S

Note: NI – no ignition; S – slow deflagration; F – fast deflagration; D – detonations.

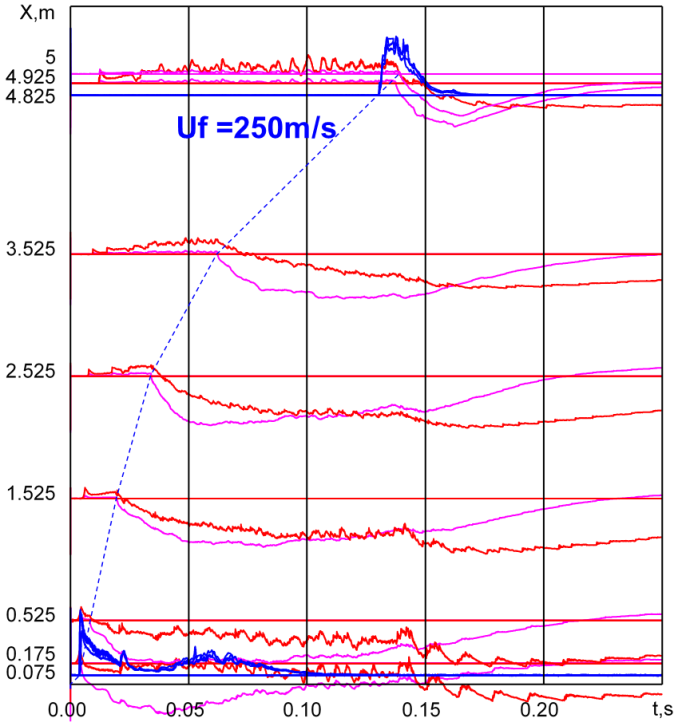

Figure 11. Distance-time diagram for subsonic deflagration of 45% vol. H_2 mixture: flame trajectory (blue dotted line); light signal (blue solid line); pressure signal (red and pink solid lines).

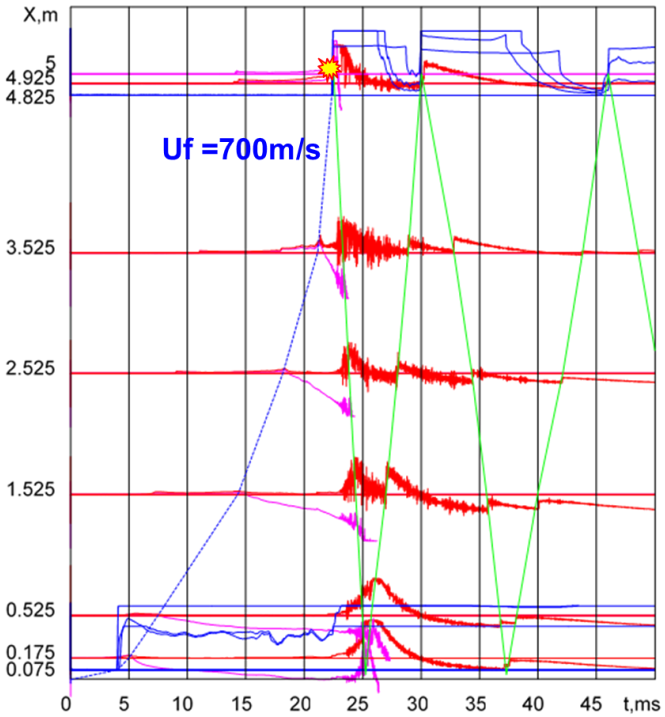

Figure 12. Distance-time diagram for sonic deflagration and detonation transition of 30% vol. H_2 mixture: flame trajectory (blue dotted line); shock wave trajectory (green line); light signal (blue solid line); pressure signal (red and pink solid lines). The star corresponds to DDT point.

For stoichiometric hydrogen air mixture (Figure 12), the flame successfully accelerates to supersonic velocity with a relatively strong shock wave which is able to initiate the detonation being reflected at the far end flange. The run-up-distance to detonation x_D = 500 λ = 5000 mm (where λ = 10 mm for stoichiometric hydrogen-air) exactly fits to the length of the tube L = 5000 mm.

All experimental data in a digital form were processed in order to evaluate characteristic flame velocity, shock wave velocity and maximum combustion pressure. The data for smooth tube experiments at ambient conditions are summarized in Table 5. The table contains an extended number of experiments including some of the preliminary tests to make the test matrix denser and to cover a wider range of hydrogen concentrations. Five "no ignition" experiments at 55% vol. H_2 and 60% vol. H_2 are not included in Table 5.

Table 5: Main experimental results for smooth tube (BR=0) and ambient temperature.

Name	%H_2	Regime	Average velocity		Maximum pressure
			$v_{P,}$	$v_{L,}$	ΔPmax, bar
PT0-30	8.1	S	0.31	0.31	0.03
PHA-03	9.07	S	0.94	1.03	0.09
PT0-29	9.2	S	0.37	0.36	0.06
PHA-02	9.46		0.82	0.82	0.06
PT0-28	10.4	S	0.44	0.44	0.06
PHA-09	10.58	S	0.75	0.76	0.16
PHA-10	11.12	S	0.43	0.44	0.14
PT0-27	11.3	S	0.48	0.50	0.07
PT0-26	12.35	S	3.24	2.51	0.22
PHA-11	12.4	S	3.49	3.59	0.34
PTN009	12.97	S	3.99	4.14	1.37
PTN016	13.94	S		2.39	1.33
PHA-05	14.6	S	9.25	14.9	0.95
PT0-01	14.8	S		6.15	0.36
PTN013	14.94	S		12.9	1.37
PTN017	14.97	S		13.7	1.33
PT0-25	15	S	3.51	8.98	0.50
PHA-12	15	S	14.2	14.7	0.92
PT0-24	15.2	S	6.6	5.77	0.47
PT0-02	19.5	S	27.3	29.6	1.82
PT0-03	19.6	S	30.6	34.3	1.98
PT0-04	19.6	S	35.9	36.3	1.96
PHA-13	20.1	S	30.2	32.5	2.02
PTN018	20.4	S		45.8	0.34
PTN005	22.5	S	74.8	74.8	1.66
PT0-06	28.2	S	122	121	2.73
PT0-05	28.4	S	147	135	1.26
PHA-14	29.1	D	1040	1073	13.9
PTN020	29.7	F	582	657	6.83
PHA-15	45.2	S	78.8	62.5	1.44
PHA-21	49.4	S	53.0	55.6	1.09

Note: NI–no ignition; S – slow deflagration; F – fast (sonic) deflagration; D – detonations

Main thermodynamic properties based on STANJAN and CELL_H2 calculations [5-6] are given in Table 6. The properties are needed to evaluate the flame propagation regimes. For hydrogen-air and hydrogen-oxygen mixtures with different diluents, a threshold between slow and fast flames corresponds to the expansion ratio of unburnt and burnt gas densities $\sigma* = 3.75$ at ambient temperature [2]. Figure 13 shows a dependence of flame propagation velocity and characteristic combustion pressure on expansion ratio for hydrogen-air mixtures in different tube diameters. The figure demonstrates that at the critical expansion ratio $\sigma*=3.75$ the velocity exceeds the speed of sound in reactants (Mach number M > 1) and the pressure exceeds the level of 2-3 bar and will be established of the order of adiabatic combustion pressure ΔP_b in case of sonic deflagration or ΔP_{CJ} in case of detonation (Table 13).

Table 6: Main thermodynamic and combustion properties of tested mixtures for smooth tube experiments (BR=0) and ambient temperature (293K).

Name	%H_2	Speed of sound		Adiabatic		Exp. ratio	Detonation		
		react.	prod.	temp.	press.		Press.	Veloc.	cell size
		cr, m/s	cp, m/s	T_b, K	P_b, bar	σ	P_{CJ}, bar	D_{CJ}, m/s	λ, mm
PT0-30	8.1	347	614	947	2.78	3.10	6.09	1184	-
PHA-03	9.07	348	637	1022	3.06	3.33	6.66	1237	16295
PT0-29	9.2	349	641	1032	3.10	3.36	6.74	1244	13489
PHA-02	9.46	349	647	1052	3.18	3.42	6.89	1258	9243
PHA-04	10.2	350	664	1108	3.38	3.59	7.31	1297	4292
PT0-28	10.4	351	668	1123	3.44	3.63	7.42	1307	3616
PHA-09	10.58	351	672	1137	3.49	3.67	7.52	1316	3099
PHA-10	11.12	352	684	1178	3.64	3.80	7.82	1342	2152
PT0-27	11.3	352	688	1191	3.69	3.84	7.92	1351	1923
PT0-26	12.35	354	711	1270	3.97	4.07	8.48	1401	1084
PHA-11	12.4	355	712	1274	3.98	4.08	8.51	1403	1058
PTN009	12.97	356	724	1316	4.13	4.20	8.81	1429	810
PTN016	13.94	357	744	1388	4.38	4.41	9.30	1472	543
PHA-05	14.6	359	757	1437	4.54	4.55	9.63	1500	420
PT0-01	14.8	359	761	1451	4.59	4.59	9.73	1508	389
PTN013	14.94	359	763	1462	4.62	4.62	9.80	1514	369
PTN017	14.97	359	764	1464	4.63	4.62	9.82	1515	365
PT0-25	15	360	765	1466	4.64	4.63	9.83	1516	361
PHA-12	15	360	765	1466	4.64	4.63	9.83	1516	361
PT0-24	15.2	360	768	1481	4.69	4.67	9.93	1525	336
PT0-02	19.5	369	847	1789	5.65	5.51	11.86	1688	56
PT0-03	19.6	369	848	1796	5.67	5.53	11.90	1691	54
PT0-04	19.6	369	848	1796	5.67	5.53	11.90	1691	54
PHA-13	20.1	370	857	1831	5.77	5.62	12.11	1708	43
PTN018	20.4	371	862	1852	5.83	5.68	12.23	1719	39
PTN005	22.5	375	895	1995	6.22	6.05	13.03	1787	22
PT0-06	28.2	389	967	2331	7.05	6.88	14.67	1943	11
PT0-05	28.4	389	969	2340	7.07	6.90	14.71	1947	10
PHA-14	29.1	391	975	2366	7.12	6.96	14.82	1962	10
PTN020	29.7	392	980	2382	7.16	7.00	14.90	1974	10
PHA-15	45.2	439	1069	2070	6.55	6.26	13.69	2143	17
PHA-21	49.4	454	1085	1952	6.23	5.96	13.05	2175	26

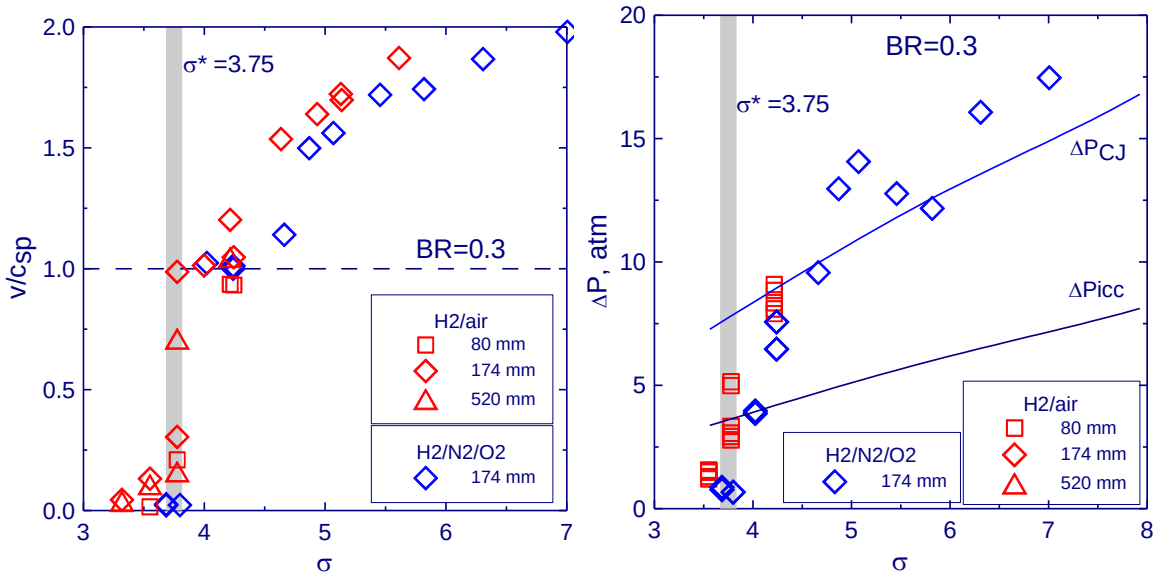

Figure 13. Characteristic velocity in Mach numbers (left) and combustion pressure (right) as function of expansion ratio for hydrogen-air and hydrogen-oxygen-nitrogen mixtures

Because for all the mixtures, except the stoichiometric one, the run-up-distance to sonic deflagration or detonation is larger than the tube length, we use obstructions with blockage ratios of 30 and 60% to reduce the run-up-distance. Figure 14 demonstrates the dependence of run-up-distance to sonic deflagration or detonation calculated [1-3] in a tube with different roughness or blockage of the channel. The dependence is based on papers [1-2] and uses the formula that takes into account the roughness or blockage of the channel and chemical reactivity of the mixture [3]. The tubes with the roughness of 5 and 50 μm can be assumed as smooth ones. Figure 14 clearly shows the efficiency of obstructions with respect to shortening the distance to sonic flame or detonation. Additionally, sonic deflagration in an obstructed tube can be stabilized as a stationary chocked flame that propagates with the speed of sound in combustion products [1-4].

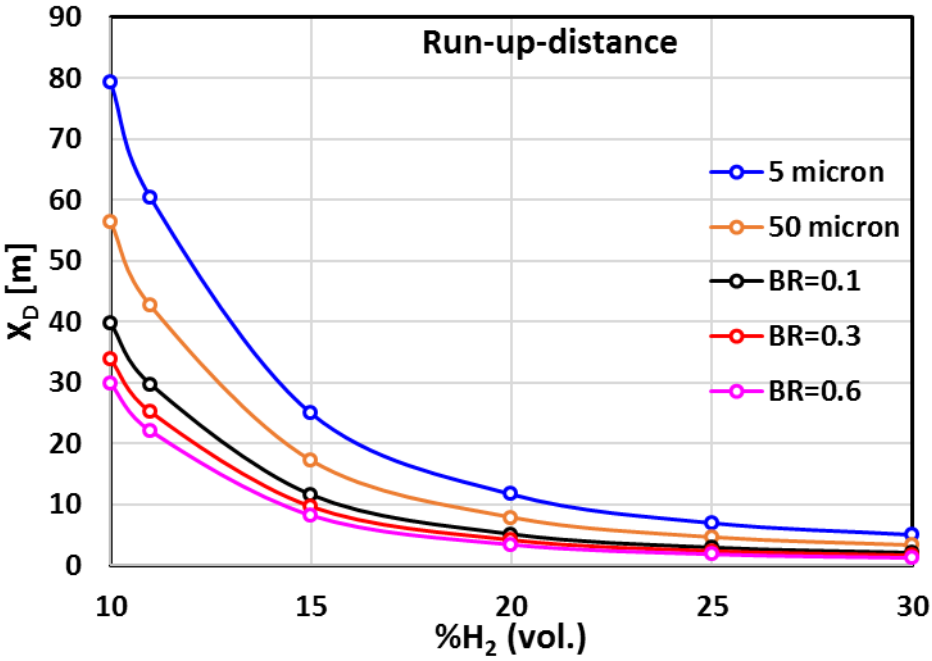

Figure 14. Calculations for run-up-distances X_D for rough/smooth and obstructed tubes.

Now, with the obstructions, we can experimentally evaluate the critical expansion ratio σ* for an efficient flame acceleration to the speed of sound because it reduces the run-up-distance almost three times. Table 7 and Table 8 summarize the main experimental results for shock tube experiments at the ambient temperature of 293 K and blockage ratio of 30%. The table contains an extended number of experiments including some of the preliminary tests to make the test matrix denser and to cover a wider range of hydrogen concentrations. Characteristic flame speed was measured using photodiodes (v_L) and pressure sensors (v_P) as shown in Figure 10 for cases where the light signal was not well resolved.

Main thermodynamic and combustion properties were calculated by STANJAN code [5] and CELL_H2 program [6] and used as a threshold for sonic flame and detonation regime evaluation. The data are given in Table 9. The speed of sound in reactants is used as a threshold for the sonic deflagration regime and the speed in between the speed of sound in products and Chapman-Jouguet detonation velocity D_{CJ} is chosen as a criterion for detonation or quasi-detonation regimes. Figure 15 confirms the critical expansion ratio σ∗=3.75 for hydrogen-air mixtures at ambient conditions. For hydrogen concentration above 11% vol. H_2 (σ=3.77) characteristic flame velocity is above the speed of sound (blue dotted line in Figure 15, right) and characteristic combustion pressure is above the adiabatic combustion pressure ΔPicc (red dotted line in Figure 15, left). For more reactive mixtures the velocity establishes at the level of speed of sound in combustion products c_p typical for chocked flames in congested areas when detonation transition is suppressed by the smaller than the detonation cell orifice diameter d=45.2 mm for BR = 30% according to papers [4, 7-9]. Really, for the mixture 19.5% vol. H_2 with detonation cell size λ > 45.2 mm, the detonation does not occur or it propagates as quasi-detonation with a velocity deficit v=1280 m/s compared to D_{CJ} = 1680 m/s. However, we distinguish the regime as quasi-detonation because characteristic flame speed is significantly higher than the speed of sound in combustion products c_p = 847 m/s. Moreover, taking into account a very big experimental discrepancy in detonation cell sizes we may tell that the real detonation cell size for 19.5 % vol. H_2 mixture is closer to 45 mm than to λ = 55 mm, as calculated by [6].

Table 7: Experiments for blockage ratio of 30% and ambient temperature.

Name	H_2, vol %	Temperature [K]	Regime
PT30-1n	14.8	293	F
PT30-2n	19.6	293	D
PT30-3n	19.6	293	D
PT30-4n	29.65	293	D
PT30-5n	29.4	293	D
PT30-6n	44.8	293	D
PT30-7n	60.0	293	NI
PT30-8n	60.0	293	NI
PT30-9n	19.5	293	D
PT30-10n	15.2	293	F
PT30-11n	12.1	293	F
PT30-12n	11.0	293	S/F
PT30-13n	10.1	293	S
PT30-14n	9.15	293	S
PT30-15n	8.15	293	S

Note: NI – no ignition; S – slow deflagration; F – fast deflagration; D – detonations

Table 8: Main experimental results for obstructed tube (BR=30%) at ambient temperature.

Name	%H_2	Regime	Average velocity		Maximum pressure
			v_P, m/s	v_L, m/s	ΔP_{max}, bar
PT30-19	7.94	S	0.20	0.36	0.13
PT30-15n	8.15	S	0.28	0.28	0.02
PT30-68	8.56	S	0.56	0.69	0.04
PT30-18	8.73	S	0.66	1.02	0.34
PT30-14n	9.15	S	0.66	0.71	0.16
PT30-67	9.5	S	0.56	0.67	0.04
PT30-13n	10.10	S	131	85.43	0.45
PT30-17	10.27	S		1.19	1.12
PT30-66	10.5	S		77.26	2.57
PT30-12n	11.00	S/F	257	287	2.52
PT30-69	11.35	S/F		201	4.01
PT30-11n	12.10	F	726	684	14.9
PT30-65	12.2	F	718	690	8.59
PT30-16	12.40	F	670	617	8.81
PT30-01n	14.8	F	892	892	23.3
PT30-71	15.1	F	729	708	12.7
PT30-10n	15.20	F	857	868	19.1
PT30-09n	19.50	F/D	1291	1251	32.5
PT30-02n	19.6	F /D	1281	1288	33.1
PT30-03n	19.6	F /D	1284	1250	29.0
PT30-05n	29.40	D	1821	1816	37.6
PT30-04n	29.65	D	1823	1770	37.8
PT30-06n	44.80	D	1880	1837	29.9
PT30-07n	60.00	NI			
PT30-08n	60.00	NI			

Note: NI – no ignition; S – slow deflagration; F – fast deflagration; D – detonations

For instance, in Ciccarelli paper [10] the detonation cell size for 20% vol. H_2 in the air is λ = 40 mm which exactly fits to the criterion of detonation onset since it is less than orifice size d = 45.2 mm. This means that we can use the criterion λ = d as a measure of detonation cell size for further experiments at cryogenic temperatures without the direct measurements of the detonation cell size.

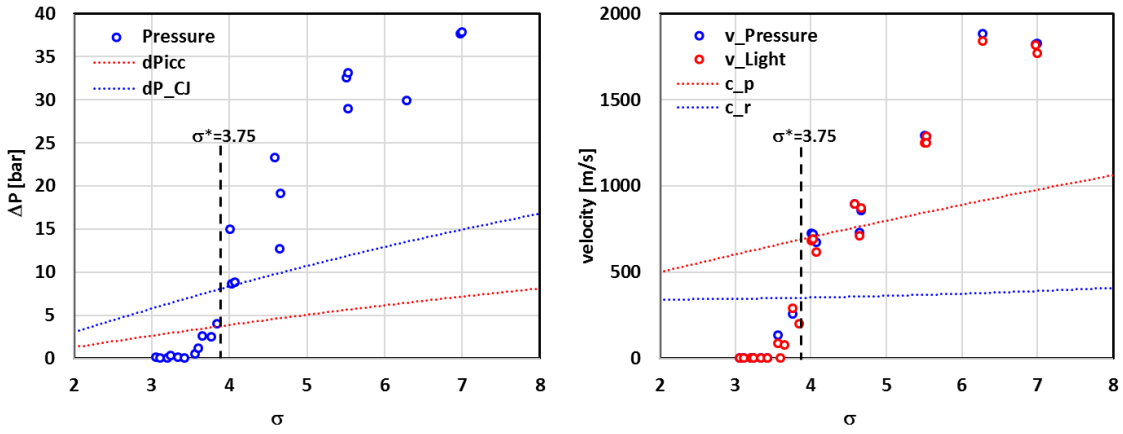

Figure 15. Characteristic pressure (left) and flame velocity (right) as function of expansion ratio at ambient conditions: black dashed line is a cut-off line at σ*=3.75.

Table 9: Main thermodynamic and combustion properties of tested mixtures for obstructed tube experiments (BR=30%) at ambient temperature (293K).

Name	%H_2	Speed of sound		Adiabatic		Exp. ratio	Detonation		
		react.	prod.	temp.	press.		Press.	Veloc.	cell size
		c_r, m/s	c_p, m/s	T_b, K	ΔP_b, bar	σ	ΔP_{CJ}, bar	D_{CJ}, m/s	λ, mm
PT30-19	7.94	346	610	935	2.73	3.06	5.99	1174	-
PT30-15n	8.15	347	615	951	2.79	3.11	6.12	1186	-
PT30-68	8.56	348	625	982	2.92	3.21	6.36	1210	48706
PT30-18	8.73	348	629	996	2.96	3.25	6.46	1219	33184
PT30-14n	9.15	349	639	1028	3.09	3.35	6.71	1242	14506
PT30-67	9.5	349	648	1055	3.19	3.43	6.91	1260	8721
PT30-13n	10.1	350	661	1100	3.36	3.57	7.25	1292	4676
PT30-17	10.27	351	665	1113	3.40	3.60	7.35	1300	4042
PT30-66	10.5	351	670	1131	3.47	3.66	7.48	1312	3319
PT30-12n	11.0	352	682	1169	3.61	3.77	7.75	1337	2319
PT30-69	11.35	353	689	1195	3.70	3.85	7.95	1354	1864
PT30-11n	12.1	354	706	1251	3.90	4.01	8.35	1389	1227
PT30-65	12.2	354	708	1259	3.93	4.03	8.40	1394	1168
PT30-16	12.4	355	712	1274	3.98	4.08	8.51	1403	1058
PT30-01n	14.8	359	761	1451	4.59	4.59	9.73	1508	387
PT30-71	15.1	360	766	1473	4.66	4.65	9.88	1520	348
PT30-10n	15.2	360	768	1481	4.69	4.67	9.93	1525	336
PT30-09n	19.5	369	847	1789	5.65	5.51	11.86	1688	56
PT30-02n	19.6	369	848	1796	5.67	5.53	11.90	1691	54
PT30-03n	19.6	369	848	1796	5.67	5.53	11.90	1691	54
PT30-05n	29.4	392	978	2375	7.14	6.99	14.86	1968	10
PT30-04n	29.65	392	980	2381	7.16	7.00	14.89	1973	10
PT30-06n	44.8	437	1067	2081	6.58	6.28	13.74	2140	17
PT30-07n	60.0	503	1125	1639	5.30	5.12	11.16	2251	148
PT30-08n	60.0	503	1125	1639	5.30	5.12	11.16	2251	148

The next series of experiments at ambient conditions was conducted in an obstructed tube with a blockage ratio BR = 60%. Table 10 and Table 11 summarize the main experimental results for shock tube experiments at the ambient temperature of 293K and the blockage ratio of 60%. Characteristic flame speed was as usually measured by applying photodiodes (v_L) and pressure sensors (v_P).

Main thermodynamic and combustion properties were calculated by STANJAN code [5] and CELL_H2 program [6] and given in Table 10. The speed of sound in reactants is used as a threshold for the sonic deflagration regime and the speed in between the speed of sound in products and Chapman-Jouguet detonation velocity D_{CJ} is chosen as a criterion for detonation or quasi-detonation regimes. Figure 16 confirms the critical expansion ratio σ*=3.75 for hydrogen-air mixtures at ambient conditions. For hydrogen concentration above 11% vol. H_2 (σ=3.77) characteristic flame velocity is above the speed of sound (blue dotted line in Figure 16, right) and characteristic combustion pressure is above the adiabatic

combustion pressure ΔPicc (red dotted line in Figure 16, left). For more reactive mixtures the velocity establishes at the level of speed of sound in combustion products c_p typical for chocked flames in congested areas when detonation transition is suppressed because the condition d >3λ for BR = 60% according to papers [4, 9] is not satisfied. The condition d =3λ for detonation onset is only satisfied for stoichiometric hydrogen-air mixture with the detonation cell size λ=9.8 mm and orifice diameter d=28.6 mm. In near critical conditions the quasi-detonation propagates with a velocity deficit v=1130 m/s compared to D_{CJ} = 1970 m/s. We classify the regime as quasi-detonation because characteristic flame speed is higher than the speed of sound in combustion products c_p = 980 m/s. The condition d >3λ for detonation onset is not satisfied for mixtures with 26.6%H2 (λ=12.1 mm) and for 45% vol. H_2 (λ=16.8 mm). This means that such conditions for BR=60% can also be used for detonation cell evaluation in combustion experiments at cryogenic temperatures.

Table 10: Experiments for blockage ratio of 60%, ambient temperature.

Name	H_2, vol %	Temperature [K]	Remarks
PT60-22	15.0	293	F
PT60-23	15.0	293	F
PT60-24	12.0	293	F
PT60-25	11.0	293	S
PT60-26	11.0	293	S
PT60-27	10.0	293	S
PT60-28	9.0	293	S
PT60-29	8.0	293	S
PT60-30	20.0	293	F
PT60-31	26.6	293	F
PT60-32	29.6	293	D
PT60-33	45.0	293	F
PT60-34	45.0	293	F
PT60-35	60.0	293	NI
PT60-36	60.0	293	NI

Note: NI – no ignition; S – slow deflagration; F – fast deflagration; D – detonations

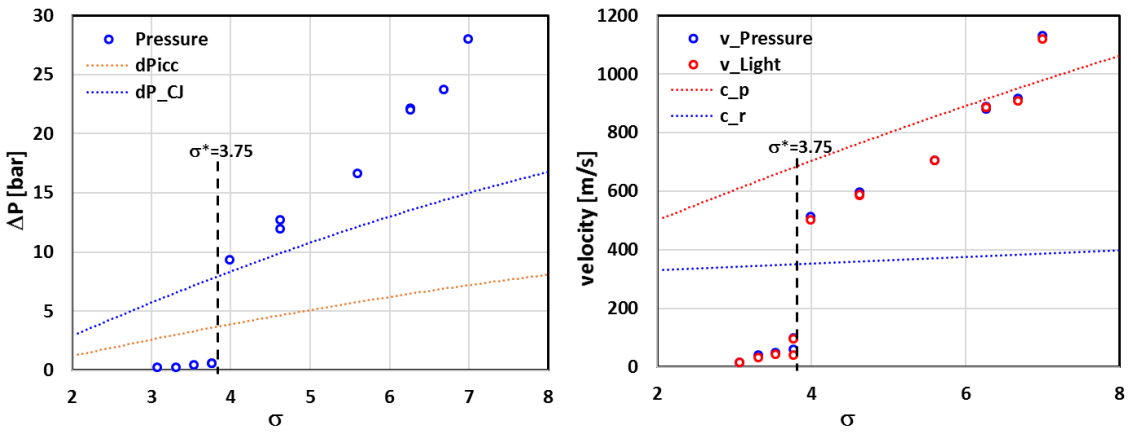

Figure 16. Experimental characteristic pressure (left) and flame velocity (right) as function of expansion ratio in obstructed tube (BR=60%) at ambient conditions.

Table 11: Main experimental results for obstructed tube (BR=60%) at T=293K.

Name	%H_2	Regime	Average velocity		Maximum pressure
			v_P, m/s	v_L, m/s	ΔPmax, bar
PT60-29	8	S	15.2	13.6	0.26
PT60-28	9	S	39.0	32.5	0.25
PT60-27	10	S	48.2	42.9	0.47
PT60-25	11	S	96.9	96.6	0.60
PT60-26	11	S	58.6	38.8	0.59
PT60-24	12	F	512	501	9.32
PT60-22	15	F	594	586	12.7
PT60-23	15	F	596	588	11.9
PT60-30	20	F	705	704	16.6
PT60-31	26.6	F	915	907	23.7
PT60-32	29.6	D	1129	1119	28.0
PT60-33	45	F	880	886	22.1
PT60-34	45	F	889	885	22.0
PT60-35	60	NI			
PT60-36	60	NI			

Note: NI – no ignition; S – slow deflagration; F – fast deflagration; D – detonations

Table 12: Main thermodynamic and combustion properties of tested mixtures for obstructed tube experiments (BR=60%) at ambient temperature (293K).

Name	%H_2	Speed of sound		Adiabatic		Exp. ratio	Detonation		
		react.	prod.	temp.	press.		Press.	Veloc.	cell size
		c_r, m/s	c_p, m/s	T_b, K	ΔP_b, bar	σ	ΔP_{CJ}, bar	D_{CJ}, m/s	λ, mm
PT60-29	8	347	612	939	2.75	3.08	6.0	1178	-
PT60-28	9	348	636	1016	3.04	3.31	6.6	1234	-
PT60-27	10	350	659	1093	3.33	3.54	7.2	1286	5095
PT60-25	11	352	682	1169	3.61	3.77	7.8	1337	2319
PT60-26	11	352	682	1169	3.61	3.77	7.8	1337	2319
PT60-24	12	354	703	1244	3.88	3.99	8.3	1384	1289
PT60-22	15	360	765	1466	4.64	4.63	9.8	1516	361
PT60-23	15	360	765	1466	4.64	4.63	9.8	1516	361
PT60-30	20	370	855	1824	5.75	5.60	12.1	1705	45
PT60-31	26.6	385	951	2250	6.86	6.68	14.3	1904	12
PT60-32	29.6	392	980	2380	7.16	7.00	14.9	1972	10
PT60-33	45	438	1068	2076	6.56	6.27	13.7	2141	17
PT60-34	45	438	1068	2076	6.56	6.27	13.7	2141	17
PT60-35	60	503	1125	1639	5.30	5.12	11.2	2251	148
PT60-36	60	503	1125	1639	5.30	5.12	11.2	2251	148

6 Experimental results. Cryogenic tests

With the current facility, it was possible to cool the tube to a well-defined cryogenic temperature. The tube was cooled down in the basin surrounding the tube with LN_2 and the experiments were conducted during the warm-up phase. It was needed about 2 hours to cool the tube down from ambient conditions to the test temperatures 90-110 K. A requirement for the test was that the temperatures shown by 6 thermocouples should not deviate too much from an average temperature in the range 90-130K. The uniformity of the temperature along the tube was monitored by thermocouples of type K at the wall inside the tube, at distances 22.5, 102.5, 103, 227, 378, 472.5 cm. Initial conditions as hydrogen concentration, temperature distribution and main results on flame propagation regimes for the smooth tube at cryogenic temperatures are collected in Table 13. We suppose the temperature of the gas mixture will be established as an average one before the test. The average temperature was established in the range 90-130 K. In some of the experiments marked with (NI) it was a problem with spark discharge at cryogenic temperatures.

Table 13: Experiments for smooth tube (BR= 0%) at cryogenic temperatures.

Name.	**H_2 [%, vol.]**	**Temperature [K]**							
		Position [cm]						**Average**	**Remarks**
		22.5	102.5	103	227	378	472.5		
PT0C-7	15.15	-	98.38	98.63	94.93	91.71	87.37	94.20	NI
PT0C-8	17	-	99.33	98.79	95.41	92.66	88.97	95.03	NI
PT0C-9	19.8	-	101.66	101.60	98.91	96.87	95.08	98.82	F
PT0C-10	18	-	99.01	97.56	97.04	93.98	93.50	96.22	NI
PT0C-11	20	-	93.44	94.00	92.70	85.31	82.74	89.64	NI
PT0C-12	19.4	-	92.68	93.03	91.59	85.82	82.28	89.08	NI
PT0C-13	20	-	97.63	93.81	91.82	88.19	85.65	91.42	NI
PT0C-14	20	-	97.48	96.39	93.55	90.66	88.42	93.30	NI
PT0C-15	20	-	97.48	96.39	93.55	90.66	88.42	93.30	NI
PT0C-16	20	-	96.52	97.24	94.39	91.74	88.98	93.77	NI
PT0C-17	19.7	-	108.48	100.01	96.36	93.73	92.35	98.18	F
PT0C-18	19.9	-	103.57	102.68	99.56	97.60	94.79	99.64	F
PT0C-19	15.1	-	105.11	104.31	101.74	100.25	97.48	101.78	NI
PT0C-20	17	-	110.14	103.94	101.70	100.06	98.49	102.87	S
PT0C-21	16.1	-	105.42	105.07	102.99	101.25	98.78	102.70	S
PT0C-22	29	107.99	105.51	102.60	101.89	99.77	98.64	101.68	D
PT0C-23	44	108.84	105.88	106.04	105.92	103.80	-	105.41	F
PT0C-31	60	106.37	-	122.62	101.88	91.47	88.65	106.14	NI
PT0C-32	45	108.10	-	116.99	103.64	95.97	91.78	106.07	D
PT0C-33	60	107.37	-	112.20	102.85	96.67	91.70	103.27	NI
PT0C-34	50	106.82	-9	109.48	102.01	96.60	92.01	102.00	F
PT0C-35	53.6	108.78	-	110.25	104.67	99.85	95.42	104.14	NI

Note: NI – no ignition; S – slow deflagration; F – fast deflagration; D – detonations.

Table 14: Main experimental results for smooth tube (BR=0) at cryogenic temperatures.

Name	H_2, % vol.	Average temperature	Regime	Average velocity		Maximum pressure
				v_P, m/s	v_L, m/s	ΔPmax, bar
PT0C-19	15.1	94.2				
PT0C-07	15.15	95.0				
PT0C-21	16.1	98.8	F	513	582	24.1
PT0C-08	17	96.2				
PT0C-20	17	89.6	F	498	480	25.3
PT0C-10	18	89.1				
PT0C-12	19.4	91.4				
PT0C-17	19.7	93.3	F/D	758	850	25.6
PT0C-09	19.8	93.3	F/D	1111	837	25.6
PT0C-18	19.9	93.8	F/D	749	823	32.1
PT0C-11	20	98.2				
PT0C-13	20	99.6				
PT0C-14	20	101.8				
PT0C-15	20	102.9				
PT0C-16	20	102.7				
PT0C-22	29	101.7	D	1390	1330	48.8
PT0C-23	44	105.4	F	705	855	39.2
PT0C-32	45	106.1	D	2113	2119	43.9
PT0C-34	50	106.1	F/D	909	897	37.5
PT0C-35	53.6	103.3				
PT0C-31	60	102.0				
PT0C-33	60	104.1				

Note: NI–no ignition; S – slow deflagration; F – fast (sonic) deflagration; D – detonations.

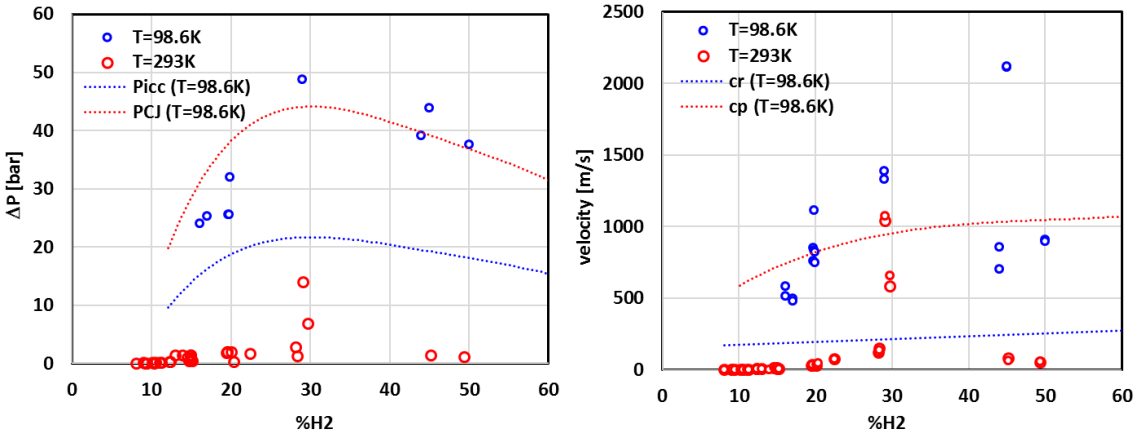

Figure 17. Experimental characteristic pressure (left) and flame velocity (right) as function of hydrogen concentration in smooth tube (BR=0%) at cryogenic and ambient temperature: experimental data (open points); theoretical calculations (dotted lines).

Main experimental results for cryogenic hydrogen combustion regimes in a smooth tube (BR=0%) are summarized in Table 14. Main thermodynamic and combustion properties were calculated by STANJAN code [5] and CELL_H2 program [6] and given in Table 15. As before, the speed of sound in reactants is used as a threshold for the sonic deflagration regime and the speed in between the speed of sound and Chapman-Jouguet detonation velocity D_{CJ} is chosen as a criterion for detonation or quasi-detonation regimes.

Table 15: Main thermodynamic and combustion properties of tested mixtures for smooth tube experiments (BR=0) at cryogenic temperatures.

Name	H_2, % vol.	To, K	Speed of sound		Adiabatic		Exp. ratio	Detonation		
			react.	prod.	temp.	press.		Press.	Veloc.	cell size
			c_r, m/s	c_p, m/s	T_b, K	ΔPb, bar	σ	ΔP_{CJ}, bar	D_{CJ}, m/s	λ, mm
PT0C-19	15.1	101.8	194.1	726	1311	14.03	11.91	28.67	1503	
PT0C-07	15.15	94.2	187.6	725	1308	15.22	12.83	31.06	1505	
PT0C-21	16.1	102.7	196.0	747	1386	14.61	12.41	29.84	1546	>170
PT0C-08	17	95.0	190.3	763	1446	16.49	13.93	33.60	1583	
PT0C-20	17	102.9	197.1	765	1453	15.21	12.92	31.03	1583	>170
PT0C-10	18	96.2	192.5	783	1521	17.00	14.38	34.63	1623	
PT0C-12	19.4	89.1	187.6	808	1617	19.44	16.39	39.52	1677	
PT0C-17	19.7	98.2	196.1	816	1646	17.80	15.12	36.23	1688	10–170
PT0C-09	19.8	98.8	196.8	818	1654	17.74	15.08	36.12	1692	10–170
PT0C-18	19.9	99.6	197.7	820	1662	17.66	15.02	35.95	1696	10–170
PT0C-11	20	89.6	188.7	820	1661	19.75	16.68	40.14	1699	
PT0C-13	20	91.4	190.4	820	1662	19.35	16.37	39.35	1699	
PT0C-14	20	93.3	192.1	820	1664	18.95	16.05	38.55	1700	
PT0C-15	20	93.3	192.1	820	1664	18.95	16.05	38.55	1700	
PT0C-16	20	93.8	192.5	820	1664	18.86	15.97	38.36	1700	
PT0C-22	29	101.7	211.1	956	2256	21.95	19.07	44.60	1987	9 – 54
PT0C-23	44	105.4	239.3	1030	1956	19.31	16.38	39.28	2137	5 – 54
PT0C-32	45	106.1	241.9	1033	1928	18.96	16.08	38.59	2144	5 – 54
PT0C-34	50	102.0	248.2	1046	1778	18.53	15.61	37.71	2174	10 – 170
PT0C-35	53.6	104.1	258.9	1056	1673	17.23	14.50	35.10	2194	
PT0C-31	60	106.1	278.6	1072	1478	15.19	12.75	31.00	2229	
PT0C-33	60	103.3	275.3	1071	1475	15.63	13.08	31.87	2228	

For some reasons, we couldn't ignite the mixtures with less than 15%H2 due to air condensation. Surprisingly, for all mixtures ignited, the flame propagated as sonic deflagration or detonation. Characteristic flame propagation velocity is at least 3-4 times higher than the speed of sound in reactants c_r at cryogenic temperatures (Figure 17, right). The maximum combustion pressure is also higher than the adiabatic combustion pressure Picc for all tested mixtures (Figure 17, left). Such data are in contradiction with warm experiments which result in sub-sonic deflagration for lean and rich hydrogen –air mixtures. Except for the stoichiometric hydrogen-air mixture, all other mixtures at ambient temperature burn very slow, with a velocity of less than 100 m/s. It corresponds to maximum combustion pressure 1-2 bar. Figure 18 and Figure 19 show a comparison of flame velocity for warm and cold experiments for different regimes of flame propagation. The figure shows that cryogenic temperatures promote the sonic flame propagation or even quasi-detonation for lean (20%H2) and rich (50%H2) hydrogen-air mixtures in comparison with ambient temperature combustion with a velocity that does not exceed the speed 80 m/s. For more reactive mixtures with 29% and 45% vol. H_2 in air the cryogenic temperatures make shorter the run-up distance to detonation compared to ambient temperatures.

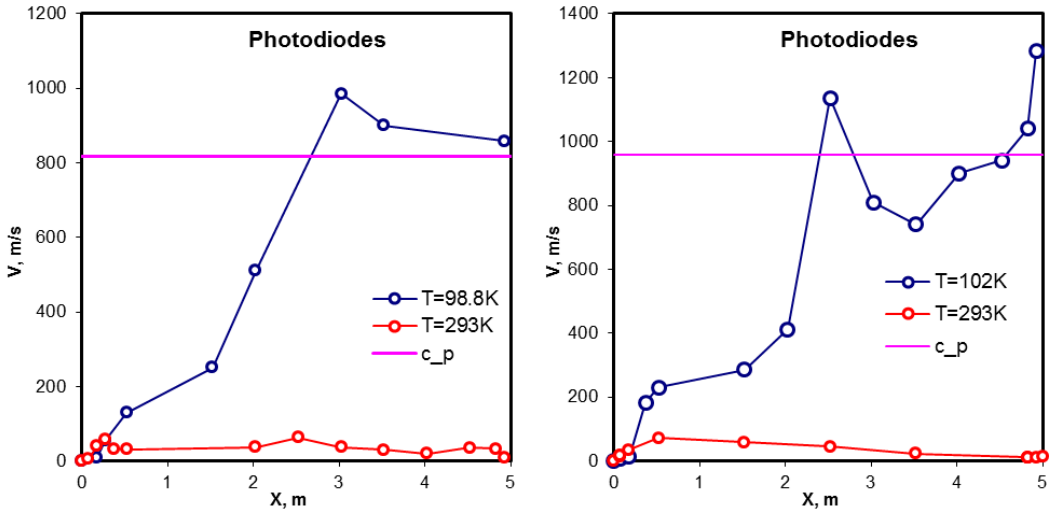

Figure 18. Comparison of flame velocity in smooth tube (BR=0%) at cryogenic and ambient temperatures: c_p is the speed of sound in combustion products; 20% vol. H_2-air (left); 50% vol. H_2-air (right).

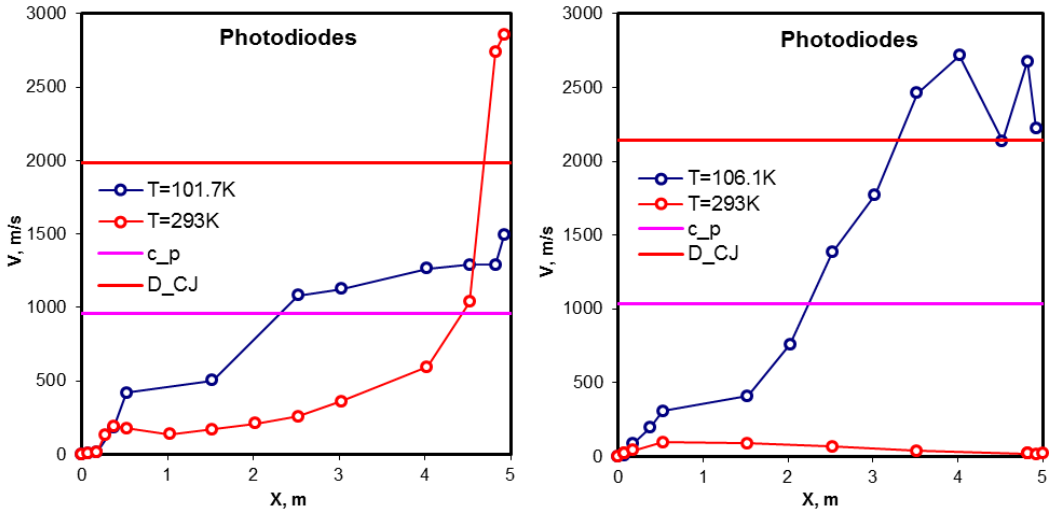

Figure 19. Comparison of flame velocity for detonation regimes in smooth tube (BR=0%) at cryogenic and ambient temperatures: c_p is the speed of sound in combustion products; 29% vol. H_2-air (left); 45% vol. H_2-air (right).

This might be due to the other reactivity of the same mixtures at cryogenic temperatures or, more probable, due to more efficient flame acceleration in more viscous and dense gas at cryogenic temperatures. Chemical reactivity cannot be higher at cryogenic temperature because the 5 times lower laminar flame speed at cryogenic temperature 100 K cannot be compensated by 3 times higher density and expansion ratio of combustion products. However, it can be compensated by 2 times lower speed of sound at cryogenic temperatures because the flame speed in terms of Mach number remains practically the same as for ambient temperature. Thus, it remains only gas dynamic properties responsible for the faster flame acceleration at cryogenic temperatures. For instance, due to 7.5 times higher kinematic viscosity at ambient conditions compared to cryogenic temperature T=100 K, the Reynolds number at cryogenic temperatures is 5 times higher to reach the threshold for sonic deflagration. It promotes the creation of turbulent flow ahead of the flame which, in turn, leads to the additional flame acceleration to sonic deflagration.

Typical x-t diagrams for cryogenic hydrogen combustion are presented in Figure 20-Figure 23 for chocked flame (16% vol. H_2), quasi-detonation (19.6% vol. H_2), detonation (45% vol. H_2) and quasi-detonation (50% vol. H_2). Among the tested mixtures, the only mixtures with 16% and 17% vol. H_2 do not exceed the speed of sound in combustion products. Figure 20 shows a stationary flame front coupled with shock wave propagating with velocity U_f = 580 m/s, slower than the speed of sound in combustion products c_p = 747 m/s. For the first time, it was discovered a stationary supersonic flame propagation (Mach number M=3) in a channel without obstacles. It might be classified as a chocked flame supported by spatial problems and energy losses. If the tube would be larger, then the detonation might occur. The critical condition for detonation propagation in a smoot channel is $d > \lambda/\pi$. Thus, we can assume that for 16% and 17% vol. H2 in air the detonation cell size $\lambda > \pi d = 170$ mm.

For mixtures from 19% to 50% vol. H_2, except the 30% and 45% vol. H_2 mixtures, a quasi-detonation regime with characteristic velocity U_f = 800-1200 m/s over the speed of sound in combustion products (M=4.3) has occurred (Figure 21 and Figure 23). Both pictures show a strong reflected shock wave. Such a regime is a transient between the chocked sonic deflagration and a quasi-detonation. The length of the tube was not enough to reach the detonation. Then, the detonation of cell size should be larger than 10 mm, but it should be less than the tube diameter to be able to propagate as a quasi-detonation. Our estimate of detonation cell sizes is given in Table 15 as lower and upper bounding limits.

For the stoichiometric hydrogen-air mixture, a quasi-detonation with velocity U_f = 1300 m/s occurs at the distance about 3.5 m and then the velocity grows to U_f = 1500-1600 m/s at the distance x_D = 4.5 m. Assuming that the run-up distance to detonation $x_D = 500 \cdot \lambda$, the detonation cell size for stoichiometric hydrogen-air at cryogenic temperature T=101.7 K is estimated to be λ = 9 mm. Since the quasi-detonation has occurred, the detonation cell size shouldn't be larger than the tube diameter (λ_{max} = d = 54 mm).

For 45% vol. H_2 a steady state detonation with the detonation velocity D = 2100 – 2400 m/s is achieved starting from the distance x_D=2.5 m (a star in Figure 22). The detonation occurs after continuous flame acceleration to speed of sound in combustion products, without a quasi-detonation stage, similar to stoichiometric hydrogen-air (29% vol. H_2). The figure shows a strong retonation wave (red dotted line) from local explosion going back to combustion products and then reflecting from the ignition end of the tube. According to [1], the run-up-distance x_D = 2.5 m leads to the lower limit of detonation cell size for 45% vol. H_2-air mixture at the temperature T=106 K is λ = 5 mm. The upper bounding limit for detonation onset in an obstructed tube for 30% and 45% vol. H_2-air mixtures at cryogenic temperature T=100 K is the detonation cell size λ = 54 mm equal to the tube diameter.

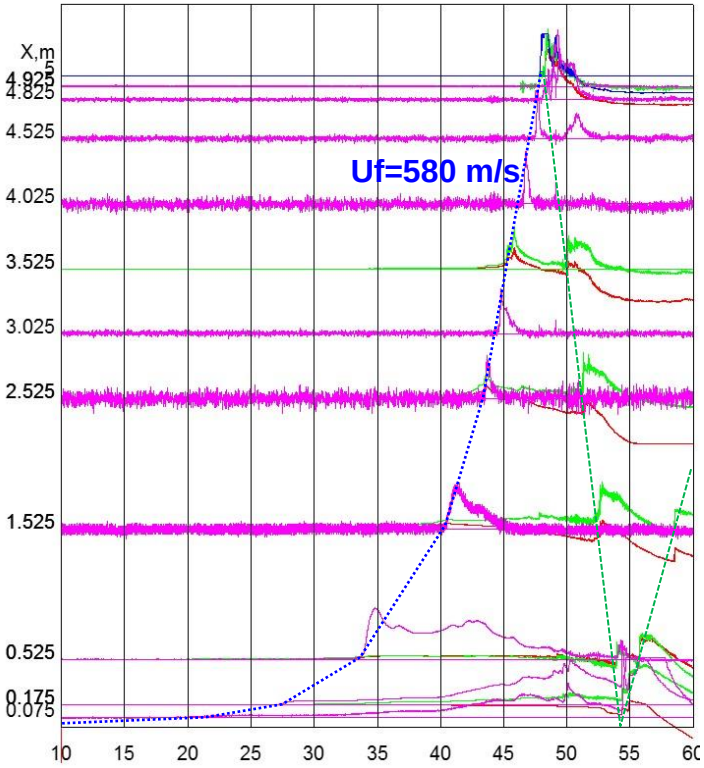

Figure 20. Distance-time diagram for sonic deflagration of 16.1% vol. H_2 at 102.7 K: flame trajectory (blue dotted line); light signal (pink solid line); pressure signal (red and green solid lines); shock wave trajectory (green dashed line)

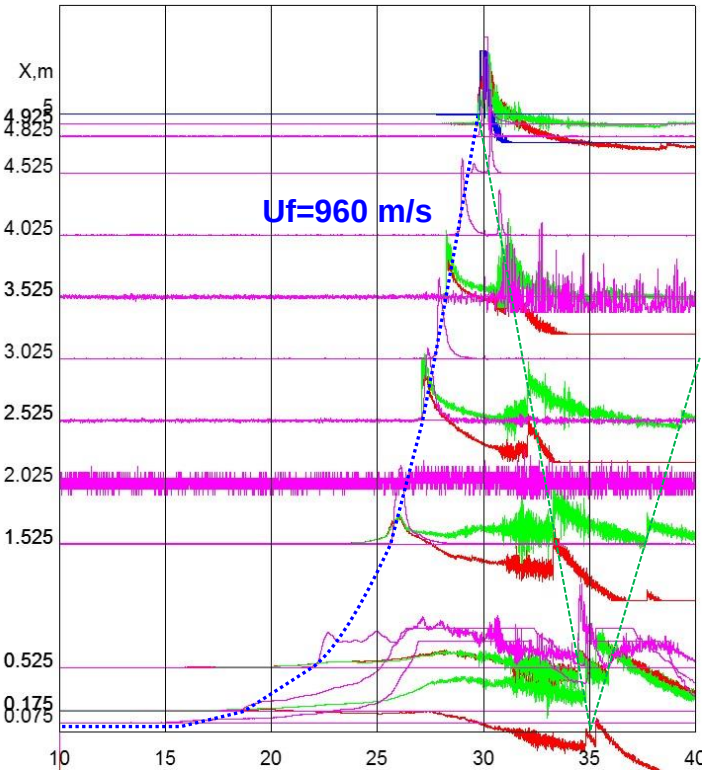

Figure 21. Distance-time diagram for sonic deflagration of 19.9% vol. H_2 at 99.6 K: flame trajectory (blue dotted line); light signal (pink solid line); pressure signal (red and green solid lines); shock wave trajectory (green dashed line).

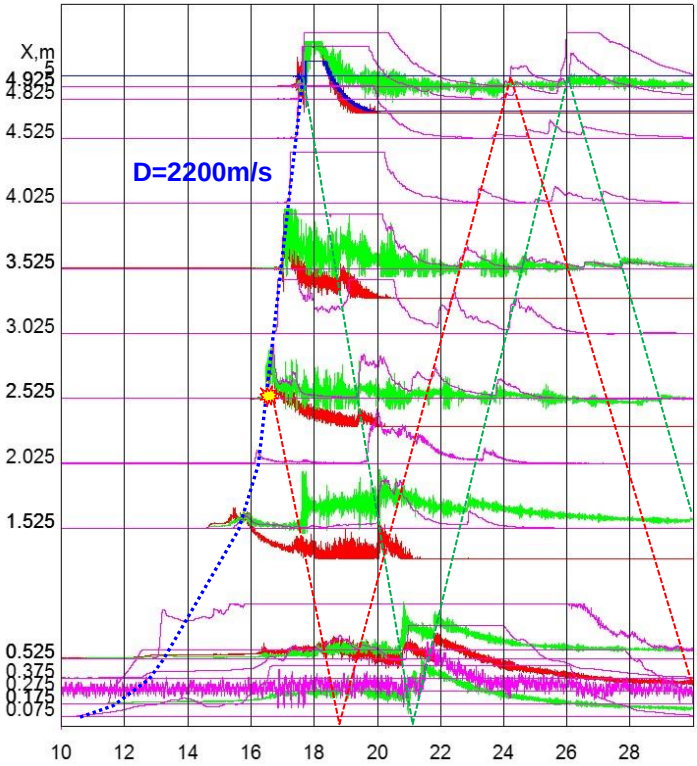

Figure 22. Distance-time diagram for detonation transition in 45% vol. H_2 (T=106 K): flame trajectory (blue dotted line); shock wave trajectory (red and green dashed lines); light signal (pink solid line); pressure signal (red and green solid lines); the star is DDT point.

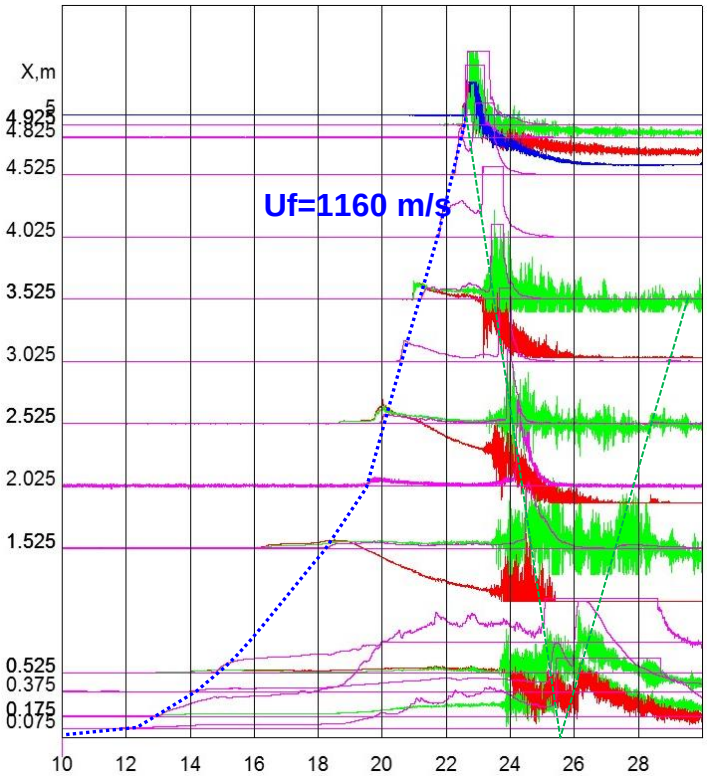

Figure 23. Distance-time diagram for sonic deflagration of 50% vol. H_2 at 102 K: flame trajectory (blue dotted line); light signal (pink solid line); pressure signal (red and green solid lines); shock wave trajectory (green dashed line)

Figure 14 shows that the blockage BR=30% decreases 2.5 times the run-up-distance to the sonic flame. It makes easier to obtain the sonic deflagration threshold for critical expansion ratio evaluation. Table 16 and summarize the main experimental results for shock tube experiments at cryogenic temperatures and blockage ratio of 30%. 21 "no ignition" experiments for very lean (8-10% vol. H_2) and for very rich (>40% vol. H_2) hydrogen-air mixtures are excluded from the tables. Nevertheless, the data on temperature distribution are available and can be presented if needed.

Table 16: Experiments at blockage ratio 30%, cryogenic temperatures.

Name	**H_2 [% vol.]**	**Temperature [K]**							**Regimes**
		Position [cm]						**Average**	
		22.5	102.5	103	227	378	472.5		
PT30C-01	15.1	129.50	137.88	135.16	135.60	114.90		130.61	F
PT30C-02	12.2	121.98	126.23	125.14	124.81	109.57		117.70	S
PT30C-04	10.3	115.67	118.39	117.63	118.39	108.04	101.29	113.23	S
PT30C-07	28.8	113.18	116.65	114.47	114.37	108.37	103.90	111.82	D
PT30C-08	28.3							111.82	D
PT30C-13	19.9							105.25	F
PT30C-24	14.95	213.58					208.03	210.80	F
PT30C-25	15.2	100.95	106.33	106.22	107.96	103.82	100.34	104.27	S
PT30C-26	12.5	102.95	106.75	106.19	107.56	104.51	101.82	104.96	S
PT30C-27	10.3	103.46	105.46	105.60	106.48	103.53	100.04	104.10	S
PT30C-30	19.7	105.22	104.02	104.46	104.46	102.00	98.12	103.05	F
PT30C-31	28.4	106.66	106.31	106.19	105.94	103.60	100.10	104.80	D
PT30C-33	34.3	108.41	107.97	108.36	108.06	105.64	101.29	106.62	D
PT30C-34	38.9	110.53	111.65	111.03	110.68	108.45	104.40	109.46	D
PT30C-36	19.85		112.50	109.57	101.19	97.33	93.59	106.88	F
PT30C-37	28		113.77	111.71	105.43	102.39	100.62	106.78	D
PT30C-38	25.5		113.50	111.36	105.85	102.78	99.96	108.71	D
PT30C-39	22.3		112.82	111.06	107.11	103.97	101.22	108.57	F
PT30C-40	15.18	114.17	112.94	111.99	108.76	105.67	102.53	109.34	S
PT30C-43	16.12	110.45	111.10	110.11	107.95	104.63	100.33	107.43	S
PT30C-44	17.8	110.03	109.89	109.64	107.74	104.31	99.94	106.92	S/F

Note: NI – no ignition; S – slow deflagration; F – fast deflagration; D – detonations.

Main thermodynamic and combustion properties calculated by STANJAN code [5] and CELL_H2 program [6] are collected in Table 18. The speed of sound in reactants is used as a threshold for the sonic deflagration regime and the speed in between the speed of sound in products and Chapman-Jouguet detonation velocity D_{CJ} is chosen as a criterion for detonation or quasi-detonation regimes. Figure 24 distinguishes the critical expansion ratio $\sigma*=12.5$ for hydrogen-air mixtures at cryogenic temperatures. For hydrogen concentration above 16% vol. H_2 ($\sigma=11.9$) characteristic flame velocity is above the speed of sound in reactants c_r (blue dotted line in Figure 24, right) and characteristic combustion pressure is above the adiabatic combustion pressure $\Delta Picc$ (red dotted line in Figure 24, left). Similar to warm tests, for more reactive mixtures the velocity establishes at the level of the speed

of sound in combustion products c_p typical for chocked flames in congested areas when the detonation transition is suppressed by the detonation cell size larger than the orifice diameter, $\lambda > d$=45.2 mm for BR = 30%, according to papers [4, 7-9]. For such mixtures, the detonation does not occur and flame propagates with the velocity v=400 – 800 m/s of the order of speed of sound in combustion products c_p = 780 – 860 m/s for mixtures with 18%-22% vol. H_2. We put the limitation of $\lambda > 45.2$ mm in Table 18 for all non-detonable mixtures. For all mixtures above 25%H2, we distinguish the regime as quasi-detonation because characteristic flame speed U_f = 1141 – 1530 m/s is significantly higher than the speed of sound in combustion products c_p = 860 - 1020 m/s but lower than CJ – detonation velocity D_{CJ} = 1890 – 2100 m/s. The limitation of $\lambda < 45.2$ mm we also put in Table 18 for all quasi-detonation and detonation regimes.

Table 17: Main experimental results for obstructed tube (BR=30%) at cryogenic temperatures.

Name	H_2, % vol.	Average temperature	Regime	Average velocity		Maximum pressure
				v_P, m/s	v_L, m/s	ΔPmax, bar
PT30C-04	10.3	113.2	S	21.3	14.5	0.80
PT30C-27	10.3	104.1	S	44.2	26.4	1.14
PT30C-02	12.2	117.7	S	95.1	73.0	1.05
PT30C-26	12.5	105.0	S	40.8	48.1	1.91
PT30C-24	14.95	210.8	F	822	863	30.5
PT30C-01	15.1	130.6	F	640	608	22.9
PT30C-40	15.18	109.3	S	111	74.7	4.03
PT30C-25	15.2	104.3	S	55	37	15.4
PT30C-43	16.12	107.4	S	47.9	54.9	6.23
PT30C-44	17.8	106.9	S/F	400	391	19.9
PT30C-30	19.7	103.1	F	758	738	39.6
PT30C-36	19.85	106.9	F	677	659	37.5
PT30C-13	19.9	105.3	F	753	737	38.1
PT30C-39	22.3	108.6	F	782	751	36.5
PT30C-38	25.5	108.7	D	1085	1142	57.5
PT30C-37	28	106.8	D	1326	1316	69.7
PT30C-08	28.3	111.8	D	1422	1416	65.1
PT30C-31	28.4	104.8	D	1370	1329	60.3
PT30C-07	28.8	111.8	D	1532	1494	
PT30C-33	34.3	106.6	D	1423	1387	62.0
PT30C-34	38.9	109.5	D	1322	1414	60.7

Note: NI–no ignition; S – slow deflagration; F – fast (sonic) deflagration; D – detonations.

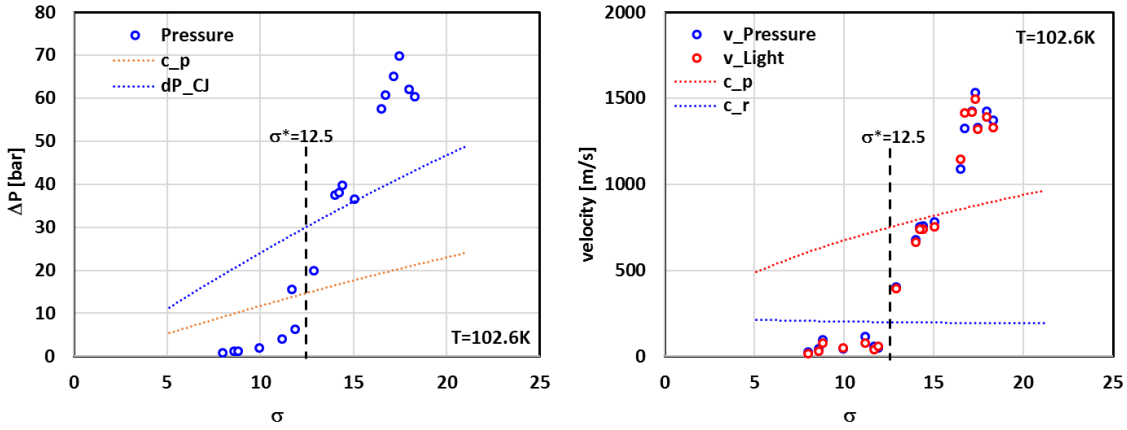

Figure 24. Experimental characteristic pressure (left) and flame velocity (right) as function of expansion ratio in obstructed tube (BR=30%) at cryogenic temperature (T=102.6K): black dashed line is a cut-off line at σ*=12.5.

Figure 25 shows a comparison of characteristic combustion pressure and velocity of the flame in the obstructed tube (BR=30%) for different hydrogen compositions at cryogenic (T = 102.6 K) and ambient temperature (T=293 K). In terms of concentration, for warm temperature, the flame accelerates to the speed of sound for leaner hydrogen-air mixtures (>11% vol. H2) than for cryogenic temperatures (>16% vol. H2). The maximum flame velocity remains almost the same for the same flame propagation regimes (slow, sonic flame or detonation). However, the maximum combustion pressure is almost two times higher at cryogenic temperature than at ambient conditions.

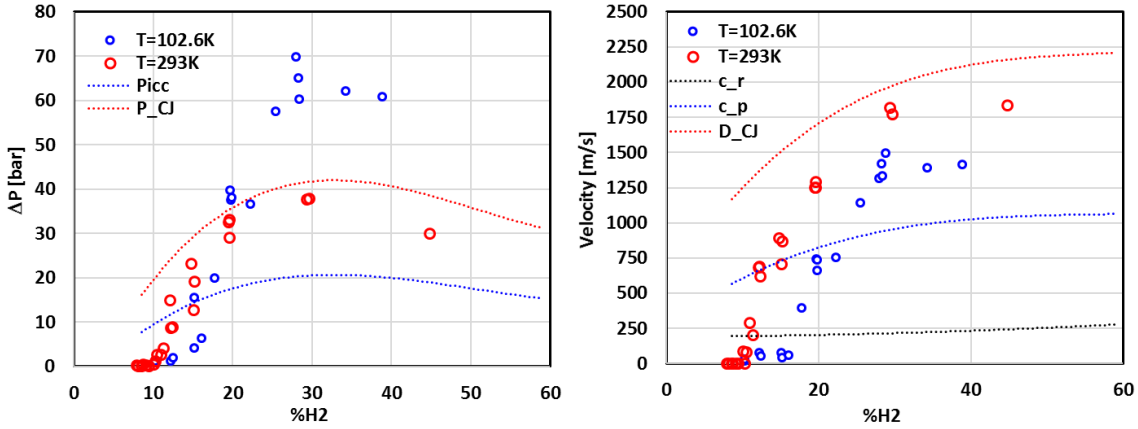

Figure 25. Experimental combustion pressure (left) and flame velocity (right) as function of hydrogen concentration in obstructed tube (BR=30%) at cryogenic and ambient temperature: experimental data (open points); theoretical calculations (dotted lines).

Typical x-t diagrams for cryogenic hydrogen combustion in the obstructed tube (BR=30%) are presented in Figure 26 - Figure 29 for slow deflagration (15.2%H2), chocked flame or sonic deflagration (17.8% and 22.3%H2), and quasi-detonation (28.3%H2). As explained in [2], below the flame acceleration limit the flame tries to accelerate but a very high level of turbulence leads to local quenching of the flame due to relatively large flame thickness and comparable size of the reaction zone and turbulent eddies. After the local quenching, the flow velocity slows down with a decreased level of turbulence. It results in the reignition of the mixture from hot combustion products and further flame acceleration. A similar process is shown in Figure 26. It looks like a galloping process of local extinction – ignition.

Each reignition and following flame acceleration lead to a pressure peak of 6 – 8 bar. Thus, the flame never exceeds the speed of sound in reactants (M <1). For more reactive mixtures, above the flame acceleration limit σ*=12.5, the flame becomes very stable, according to Borghi diagram [2], because of smaller flame thickness and it can withstand the turbulence without an extinction. Even, the turbulence produced by the interaction of the flow with obstacles promotes the further flame acceleration to the speed of sound in combustion products. For mixtures up to 22%H2 with λ > d =45.2 mm (for BR=30%) the flame stationary propagates with velocity 400 – 800 m/s (Figure 27 and Figure 28). For mixtures with λ < d =45.2 mm, the flame propagates as a quasi-detonation (Figure 29).

Table 18: Main thermodynamic and combustion properties of tested mixtures for obstructed tube (BR=30%) at cryogenic temperatures.

Name	%H_2	To, K	Speed of sound		Adiabatic		Exp. ratio	Detonation		
			react.	prod.	temp.	press.		Press.	Veloc.	cell size
			c_r, m/s	c_p, m/s	Tb, K	ΔPb, bar	σ	ΔP_{CJ}, bar	D_{CJ}, m/s	λ, mm
PT30C-04	10.3	113.23	198	619	955	9.2	8.00	19.0	1275	
PT30C-27	10.3	104.10	191	617	946	10.0	8.62	20.7	1273	
PT30C-02	12.2	117.70	204	666	1105	10.2	8.82	21.0	1372	
PT30C-26	12.5	104.96	194	669	1117	11.7	9.98	24.0	1385	
PT30C-24	14.95	210.80	326	746	1393	6.6	6.11	13.7	1507	
PT30C-01	15.1	130.61	217	732	1336	10.9	9.45	22.3	1506	
PT30C-40	15.18	109.34	201	729	1323	13.1	11.18	26.8	1508	
PT30C-25	15.2	104.27	196	728	1320	13.8	11.70	28.1	1508	
PT30C-43	16.12	107.43	200	748	1392	14.0	11.91	28.6	1547	
PT30C-44	17.8	106.92	202	781	1515	15.1	12.91	30.9	1616	λ > 45.2
PT30C-30	19.7	103.05	200	816	1650	16.9	14.44	34.5	1689	λ > 45.2
PT30C-36	19.85	106.88	204	820	1664	16.4	14.03	33.4	1694	λ > 45.2
PT30C-13	19.9	105.25	203	821	1666	16.7	14.26	34.0	1696	λ > 45.2
PT30C-39	22.3	108.57	208	863	1839	17.5	15.06	35.7	1783	λ > 45.2
PT30C-38	25.5	108.71	213	915	2057	19.1	16.53	38.9	1888	λ < 45.2
PT30C-37	28	106.78	217	947	2211	20.1	17.47	40.8	1961	λ < 45.2
PT30C-08	28.3	111.82	219	951	2229	19.7	17.18	40.1	1968	λ < 45.2
PT30C-31	28.4	104.80	213	951	2229	21.1	18.32	42.9	1972	λ < 45.2
PT30C-07	28.8	111.82	220	956	2253	19.8	17.33	40.4	1980	λ < 45.2
PT30C-33	34.3	106.62	224	999	2221	20.9	17.98	42.6	2066	λ < 45.2
PT30C-34	38.9	109.46	234	1016	2102	19.6	16.75	39.9	2103	λ < 45.2

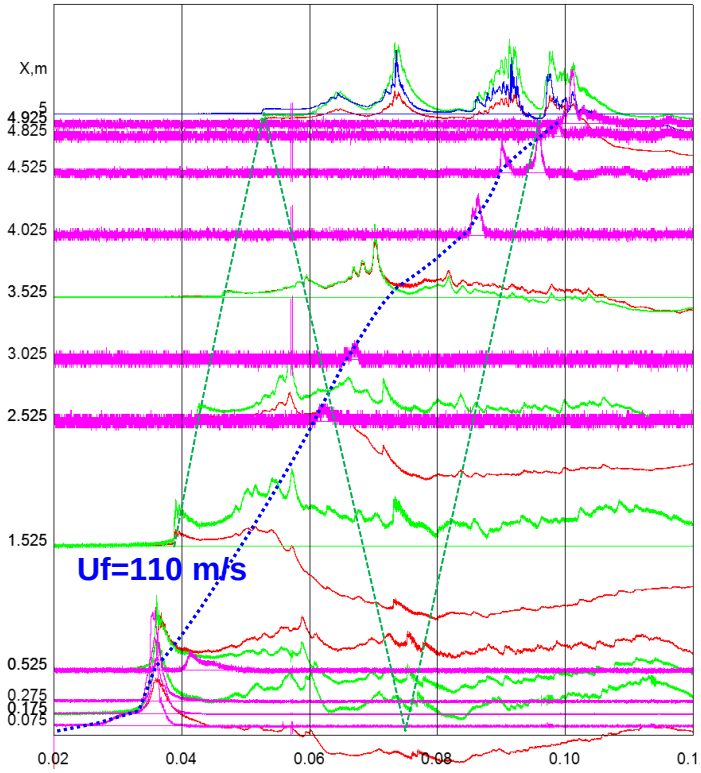

Figure 26. Distance-time diagram for slow deflagration of 15.2% vol. H_2 at 109.3 K: flame trajectory (blue dotted line); light signal (pink solid line); pressure signal (red and green solid lines); shock wave trajectory (green dashed line).

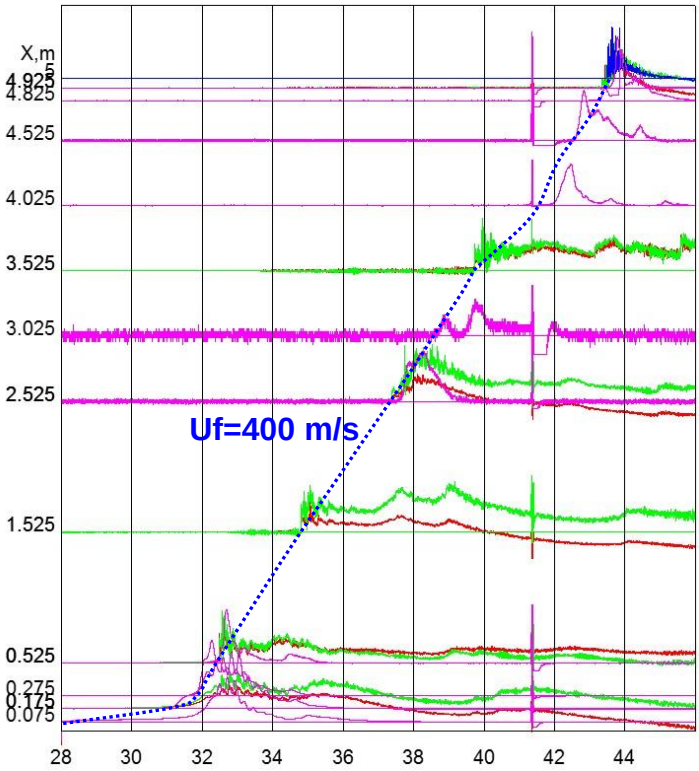

Figure 27. Distance-time diagram for sonic deflagration of 17.8% H_2 at 106.9 K: flame trajectory (blue dotted line); light signal (pink solid line); pressure signal (red and green solid lines).

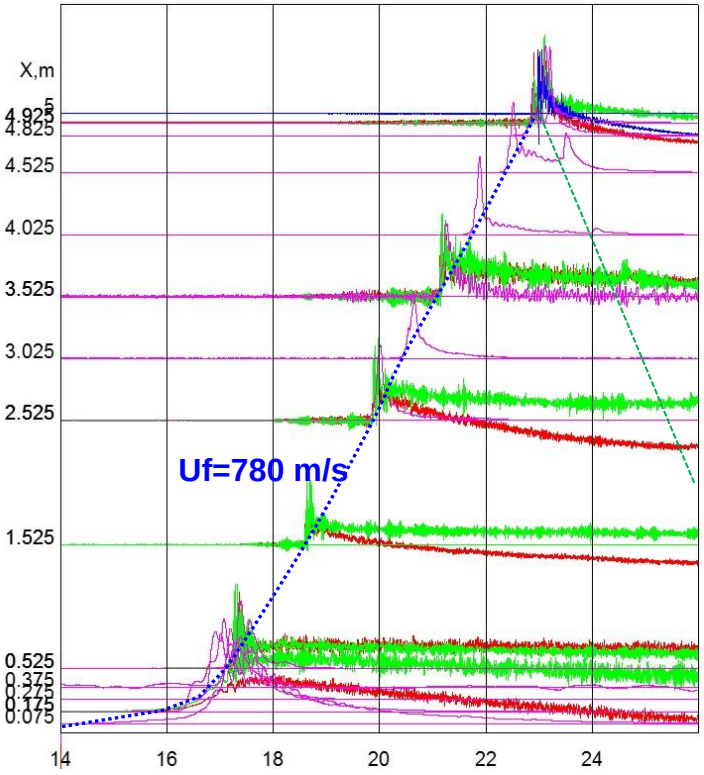

Figure 28. Distance-time diagram for sonic deflagration of 22.3% vol. H_2 at 108.6 K: flame trajectory (blue dotted line); light signal (pink solid line); pressure signal (red and green solid lines); shock wave trajectory (green dashed line).

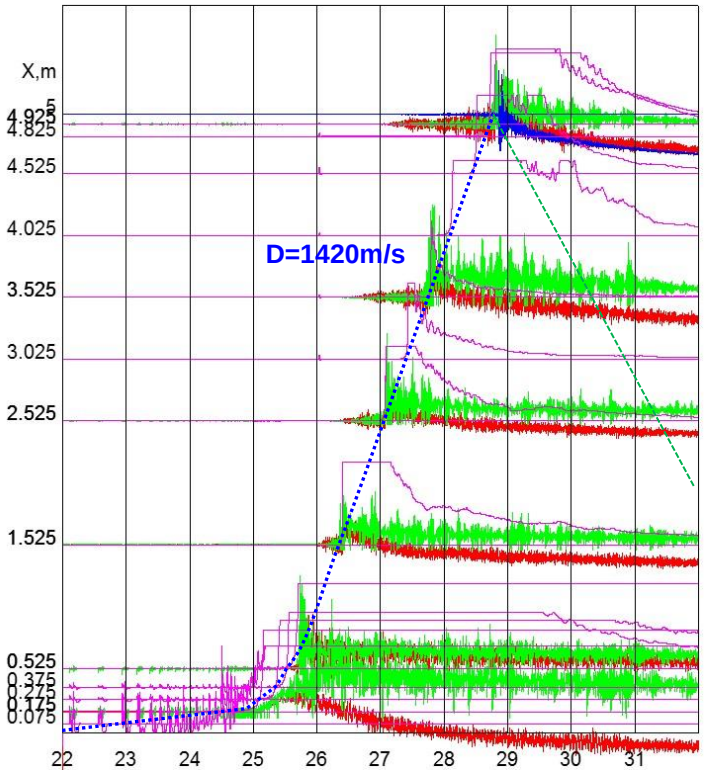

Figure 29. Distance-time diagram for quasi-detonation in 28.3% vol. H_2 (T=111.8 K): flame trajectory (blue dotted line); shock wave trajectory (green dashed lines); light signal (pink solid line); pressure signal (red and green solid lines).

Figure 30 summarizes the current experimental data on flame propagation regimes in a tube with obstacles blocked in 30% (BR=30%). The critical expansion ratio for flame acceleration to the speed of sound can be approximated by exponential function:

$$\sigma^* = 2400 \cdot T^{-1.12} \qquad (2)$$

where T is the initial temperature. Approximation (2) covers the range of temperatures from 90 K to 300 K. As follows from paper [2], the critical expansion ratio is not sensitive to the blockage of the channel and shape of the obstacles. We expect it should be the same critical expansion ratio σ* at cryogenic temperatures for larger blockage BR=60%, similar to warm experiments at T=293 K. The validity of the critical expansion ratio obtained in a channel with obstacles was also confirmed for high pressure hydrogen jet ignition [11].

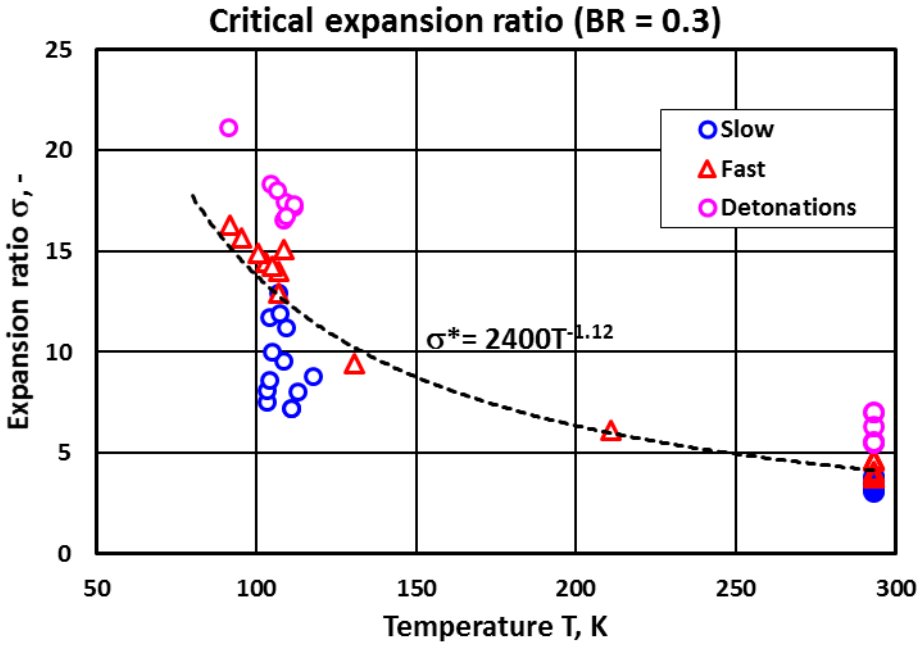

Figure 30. Critical expansion ratio as function of initial temperature based on experiments in obstructed tube (BR=30%).

A series of experiments with a higher blockage ratio BR=60% was conducted at cryogenic temperatures. The series of experiments with different blockage should confirm our previous finding of the critical expansion ratio σ* = 12.5 for BR=30% at T = 100 K and reduce the bounding values for detonation cell sizes evaluated in the tests with blockage ratios 0 and 30% (Table 15 and Table 18). Table 19 and Table 20 summarize the main experimental results for shock tube experiments at cryogenic temperatures and blockage ratio BR = 60%. The main thermodynamic and combustion properties of tested mixtures are collected in Table 21. As in previous chapters, the speed of sound in reactants c_r is used as a threshold for the sonic deflagration regime and the speed in between the speed of sound in products c_p and Chapman-Jouguet detonation velocity D_{CJ} is chosen as a criterion for detonation or quasi-detonation regimes. Figure 31 confirms the same critical expansion ratio σ*=12.5 for hydrogen-air mixtures at cryogenic temperatures in a tube with blockage BR = 60%. The figure shows that for hydrogen concentration above 15.3% vol. H_2 (σ=12.95) characteristic flame velocity exceeds the speed of sound in reactants (blue dotted line in Figure 31, right) and characteristic combustion pressure is above the adiabatic combustion pressure ΔPicc (red dotted line in Figure 31, left).

Table 19: Experiments at blockage ratio 60%, cryogenic temperatures.

Name	H_2 [% vol.]	Temperature [K]							Regime
		Position [cm]						Average	
		22.5	102.5	103	227	378	472.5		
PT60C-37	15.4		106.30	105.21		107.39	97.59	104.12	NI
PT60C-38	12.5							94.45	S
PT60C-39	11.1		97.59	98.67		95.41	86.15	94.45	S
PT60C-41	10.1		98.28	99.15		96.36	89.82	95.90	S
PT60C-42	9.2		95.41	95.41		95.41	88.87	93.77	S
PT60C-44	8.1		95.49	95.04		94.59	90.01	93.78	S
PT60C-45	20.5		94.90	93.88		93.75	90.71	93.78	NI
PT60C-46	29.4		94.86	96.40		94.61	90.08	93.31	F
PT60C-47	29.7		98.87	97.34		96.46	93.81	93.99	F
PT60C-48	45		101.26	99.22		98.56	94.13	96.62	F
PT60C-49	58.5		100.85				89.96	98.29	NI
PT60C-50	15.3	96.82	98.14	97.12	96.76	91.10	84.27	95.41	F
PT60C-51	19.4	99.29	99.81	98.51	98.22	94.22	86.80	94.04	F
PT60C-52	53.8	97.62	98.04	97.57	97.06	91.66	86.03	96.14	NI
PT60C-53	51.3	98.13	96.60	97.12	96.72	93.78	84.79	94.66	F
PT60C-54	19.7	100.52	99.19	99.09	98.64	96.13	88.11	94.52	F
PT60C-55	9.1	99.57	97.80	97.77	97.25	94.93	87.91	96.95	S
PT60C-56	8.05	99.24	97.29	97.43	96.95	94.92	87.65	95.87	S

Note: NI – no ignition; S – slow deflagration; F – fast deflagration; D – detonations.

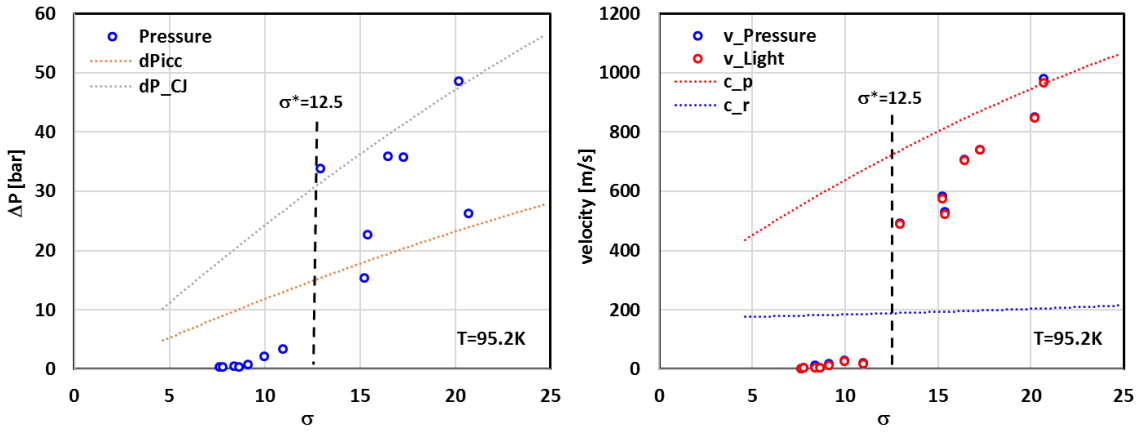

Figure 31. Experimental characteristic pressure (left) and flame velocity (right) as function of expansion ratio in obstructed tube (BR=60%) at ambient conditions: black dashed line is a cut-off line at σ*=12.5.

Table 20: Main experimental results for obstructed tube (BR=60%) at cryogenic temperatures.

Name	H_2, % vol.	Average temperature	Regime	Average velocity		Maximum pressure
				v_P, m/s	v_L, m/s	ΔPmax, bar
PT60C-56	8.05	95.6	S	2.61	1.37	0.37
PT60C-44	8.1	93.8	S	5.22	4.04	0.33
PT60C-55	9.1	95.9	S	12.9	4.05	0.44
PT60C-42	9.2	93.8	S	5.03	4.15	0.39
PT60C-41	10.1	95.9	S	17.7	12.1	0.72
PT60C-39	11.1	94.5	S	27.6	26.3	2.13
PT60C-38	12.5	94.5	S	21.4	17.4	3.38
PT60C-50	15.3	94.0	F	491	490	33.7
PT60C-37	15.4	104.1	NI			
PT60C-51	19.4	96.1	F	582	575	15.4
PT60C-54	19.7	96.2	F	529	521	22.6
PT60C-45	20.5	93.3	NI			
PT60C-46	29.4	94.0	F	980	965	26.2
PT60C-47	29.7	96.6	F	850	847	48.5
PT60C-48	45	98.3	F	740	739	35.7
PT60C-53	51.3	94.5	F	707	702	35.9
PT60C-52	53.8	94.7	NI			
PT60C-49	58.5	95.4	NI			

Note: NI–no ignition; S – slow deflagration; F – fast (sonic) deflagration; D – detonations

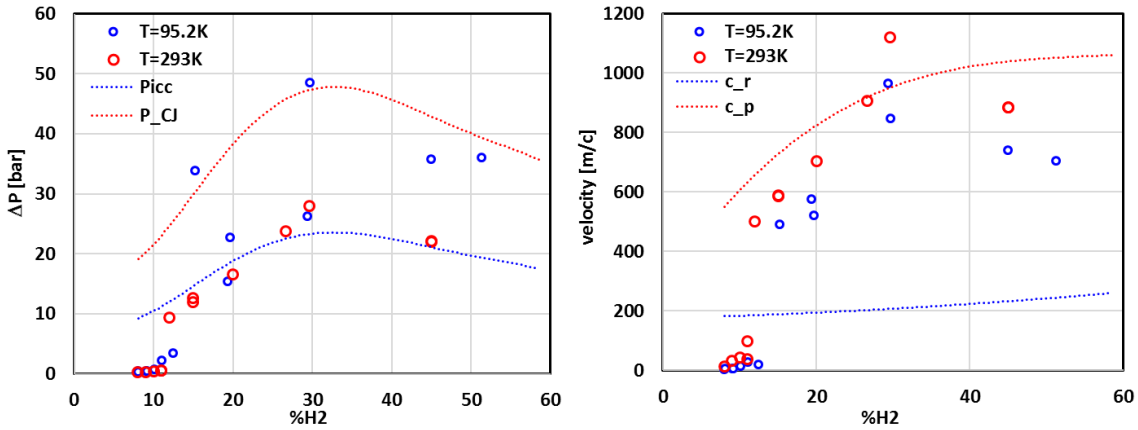

Figure 32. Comparison of experimental combustion pressure (left) and flame velocity (right) in obstructed tube (BR=60%) at cryogenic and ambient temperature: experimental data (open points); theoretical calculations only for cryogenic temperatures (dotted lines).

Characteristic orifice size for BR=60% d = 28.6 mm is almost two times less than the tube inner diameter D = 54 mm. It makes easier the flame acceleration due to the flow velocity increase within the orifice but it brings spatial problems for detonation onset. The run-up-distance to flame acceleration to the speed of sound in the obstructed tube with BR=60% is 3 times shorter than that in a smooth tube. As confirmed in the series of warm tests for the same blockage ratio, the detonation transition is suppressed by energy losses because the orifice diameter d = 28.6 mm is less than the triple detonation cell size $d < 3\lambda$ for BR =

60%, according to papers [4, 9]. So that the detonation cell size for all mixtures tested at cryogenic temperatures is larger than λ = 9.5 mm. The limitation of λ > 9.5 mm we may put in Table 21 for all non-detonable mixtures.

Table 21: Main thermodynamic and combustion properties of tested mixtures for obstructed tube (BR=60%) at cryogenic temperatures.

Name	%H_2	To, K	Speed of sound		Adiabatic		Exp. ratio	Detonation		
			react.	prod.	temp.	press.		Press.	Veloc.	cell size
			cr, m/s	cp, m/s	Tb, K	ΔPb, bar	σ	ΔP_{CJ}, bar	D_{CJ}, m/s	λ, mm
PT60C-56	8.05	95.6	181.7	554	761	8.88	7.64	18.36	1143	
PT60C-44	8.1	93.8	180.2	555	763	9.11	7.81	18.81	1145	
PT60C-55	9.1	95.9	182.9	583	844	9.84	8.41	20.28	1205	
PT60C-42	9.2	93.8	181.2	585	850	10.16	8.65	20.92	1210	
PT60C-41	10.1	95.9	183.9	609	923	10.75	9.14	22.09	1261	
PT60C-39	11.1	94.5	183.7	634	1000	11.81	10.00	24.22	1313	
PT60C-38	12.5	94.5	185.1	667	1108	13.02	10.99	26.65	1383	
PT60C-50	15.3	94.0	187.6	728	1319	15.37	12.95	31.36	1511	λ > 9.5
PT60C-37	15.4	104.1	196.4	733	1335	13.92	11.84	28.45	1517	
PT60C-51	19.4	96.1	194	810	1623	17.98	15.24	36.60	1677	λ > 9.5
PT60C-54	19.7	96.2	194.4	815	1645	18.16	15.41	36.97	1688	λ > 9.5
PT60C-45	20.5	93.3	192.7	829	1700	19.29	16.35	39.23	1718	
PT60C-46	29.4	94.0	204.4	959	2266	23.94	20.70	48.58	1997	λ > 9.5
PT60C-47	29.7	96.6	207.3	962	2276	23.33	20.21	47.36	2003	λ > 9.5
PT60C-48	45	98.3	233.9	1032	1921	20.50	17.29	41.67	2144	λ > 9.5
PT60C-53	51.3	94.5	242.9	1048	1734	19.67	16.46	39.99	2181	λ > 9.5
PT60C-52	53.8	94.7	248.8	1054	1658	18.94	15.82	38.51	2195	
PT60C-49	58.5	95.4	261.7	1066	1515	17.40	14.50	35.42	2220	

Figure 33 summarizes the current experimental data on flame propagation regimes in a tube blocked in 60% (BR=60%). The critical expansion ratio for flame acceleration to the speed of sound can be approximated by exponential function:

$$\sigma^* = 2200 \cdot T^{-1.12}, \qquad (3)$$

where T is the initial temperature in Kelvin. Function (3) covers the range of temperatures from 90 K to 300 K. The points for warm experiments with a tube blocked in 60% are not shown in Figure 33. But the correlation Eq. (3) gives the critical expansion ratios σ* = 3.79 (for T = 293 K) and σ* = 12.66 (for T = 100 K) very close to experimental values σ* = 3.75 and σ* = 12.5, respectively. The experiments for BR = 60% demonstrate the same critical expansion ratios as for BR = 30% and might be used for flame acceleration assessment in different geometries.

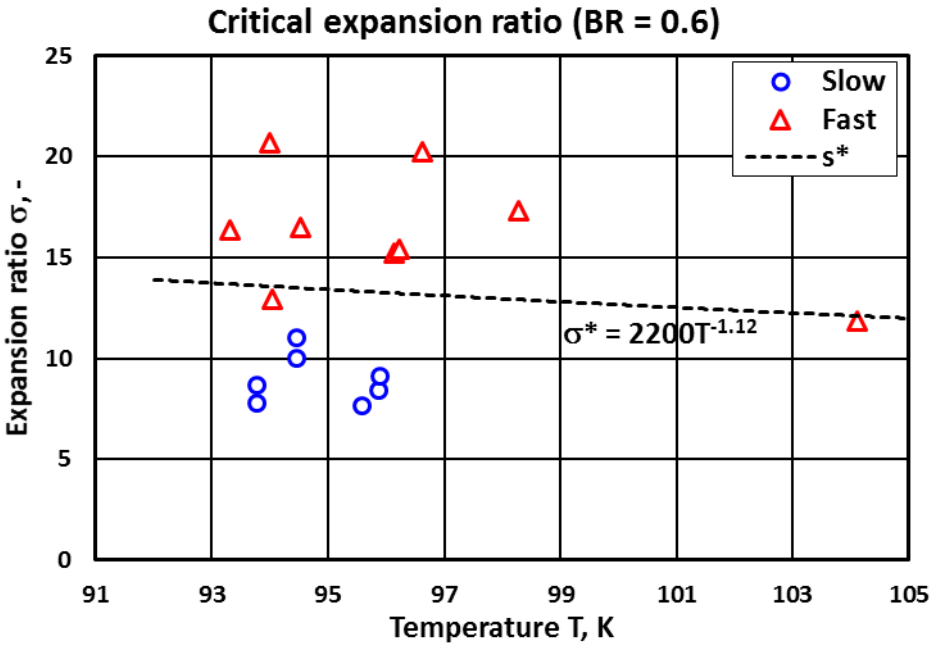

Figure 33. Critical expansion ratio as function of initial temperature based on experiments in obstructed tube (BR=60%).

Typical x-t (distance-time) diagrams for cryogenic hydrogen combustion in the obstructed tube (BR=60%) are presented in Figure 34 and Figure 35 for slow deflagration (12.5%H2) and chocked flame or sonic deflagration (45%H2). The flame for 12.5% vol. H_2 has no potential to accelerate to the speed of sound because the expansion ratio of the mixture σ = 11 is less than the critical expansion ratio σ^* = 12.5. Below the flame acceleration limit even with obstacles, the flame initially propagates with velocity 3-5 m/s and then accelerates to 32 m/s to the middle of the tube. The maximum combustion pressure does not exceed 2 bar. Then developing turbulence suppresses the flame acceleration due to local extinction. After the flow velocity slows down to U_f = 9 m/s, the flame reignites from the hot combustion products and again accelerates. At this moment, the local combustion pressure may reach 5-6 bar. Such repeatable extinction – ignition mechanism is described in [2]. Each reignition and following flame acceleration lead to the pressure peak of 5 – 6 bar. In general, the flame never exceeds the speed of sound in reactants (M <1). For a more reactive mixture of 45% vol. H_2 with the expansion ratio σ=17.3, above the flame acceleration limit σ^*=12.5, the flame is stable according to the Borghi diagram [2], because of the smaller flame thickness and it can withstand to the turbulence without an extinction. The turbulence produced by the interaction of the flow with obstacles promotes the flame acceleration to the speed U_f=740 m/s. Because of energy losses in the highly obstructed channel at BR=60%, the actual flame velocity is 25% lower than the speed of sound in combustion products c_p = 1040 m/s. The flame accelerates very quickly, after 3-4 obstacles, with x_D = 15-20 cm. Then, it stationary propagates along the whole channel as a chocked flame with a velocity about 740 m/s producing a peak pressure of 40-50 bar. Such level of pressure for sonic deflagration is even higher than the CJ-detonation pressure ΔP_{CJ} = 41.7 bar because of the shock reflection with obstacles. Spatial problems do not allow the detonation transition even for the stoichiometric mixture. This means that the detonation cell size for all mixtures tested at cryogenic temperatures about T = 100 K is above λ =9.5 mm according to the criterion d >3λ because the orifice size for BR = 60% d = 28.6 mm.

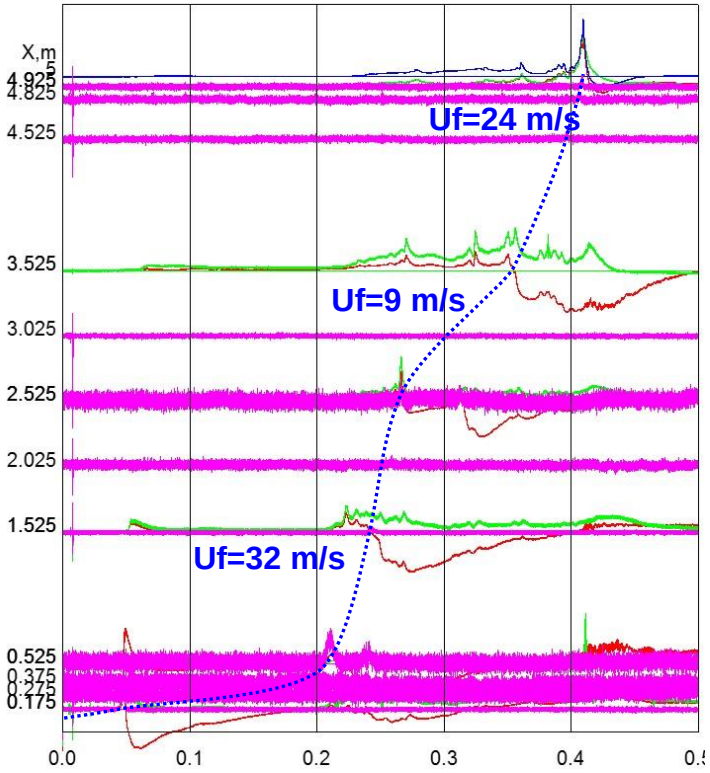

Figure 34. Distance-time diagram for slow deflagration of 12.5% vol. H_2 at 94.5 K: flame trajectory (blue dotted line); light signal (pink solid line); pressure signal (red and green solid lines).

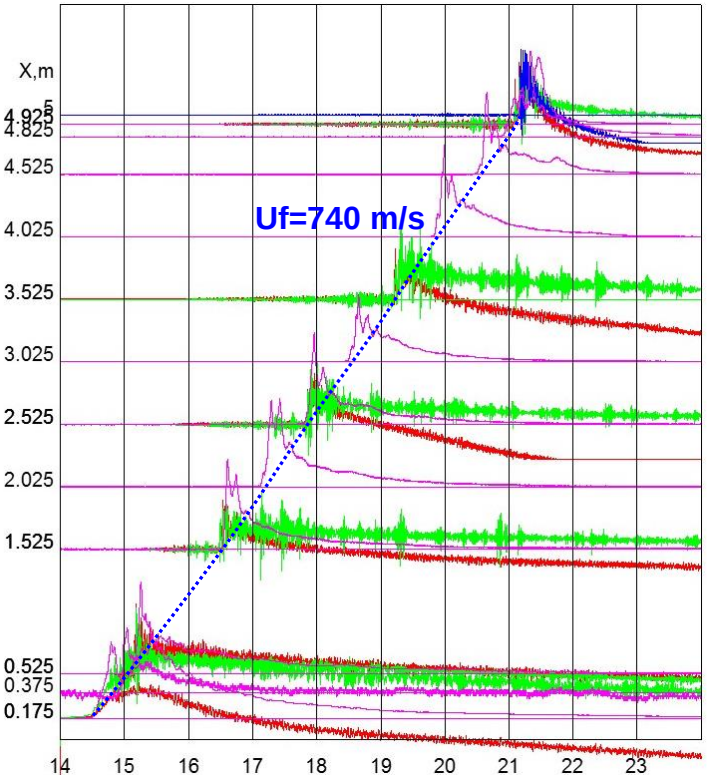

Figure 35. Distance-time diagram for sonic deflagration of 45% vol. H_2 at 94.1 K: flame trajectory (blue dotted line); light signal (pink solid line); pressure signal (red and green solid lines).

7 Discussion.

This chapter is dedicated to the analysis of all experimental data with respect to develop the criteria for effective flame acceleration and detonation transition. We also summarize the main combustion properties to assess the danger of cryogenic hydrogen combustion for humans and structures of LH2 infrastructure.

Integral combustion characteristics are the maximum combustion pressure and characteristic flame propagation velocity established in the main combustion process. Based on gas dynamic relationship and considering the flame as a piston propagation with the flame velocity, there is a dependence of dynamic pressure against the flow velocity:

$$\frac{P_2}{P_1} = \frac{2\gamma}{\gamma+1} M^2 - \frac{\gamma-1}{\gamma+1}, \qquad (4)$$

where P_2 is the dynamic combustion pressure in our case; P_1 is the initial pressure 1 bar; γ is the adiabatic coefficient of burned composition; $M = v/c$ is the Mach number as a ratio of flow (fame) velocity $v = U_f$ over the speed of sound reactants $c = c_r$. Figure 36 shows the difference of dynamic pressure at cryogenic temperature T = 100 K in comparison with ambient initial temperature for the same stoichiometric hydrogen-air mixture. Dynamic pressure at cryogenic temperature is 2-3 times higher than at ambient temperature for the same flow velocity. The reasons are almost two times lower speed of sound and larger adiabatic coefficient at cryogenic temperature. Such behaviour was experimentally confirmed in current experiments for different tube geometry Figure 37, Figure 38, and Figure 39. It was shown that maximum combustion pressure at the temperature T = 100 K is about 2 times higher than at ambient temperature. It is of practical interest that the dependence pressure vs. flame velocity is practically linear. Theoretically, the overpressure of about 2.6 bar corresponds to the flow speed with the speed of sound (M = 1). This is the main reason to prevent fast sonic deflagration for safety applications.

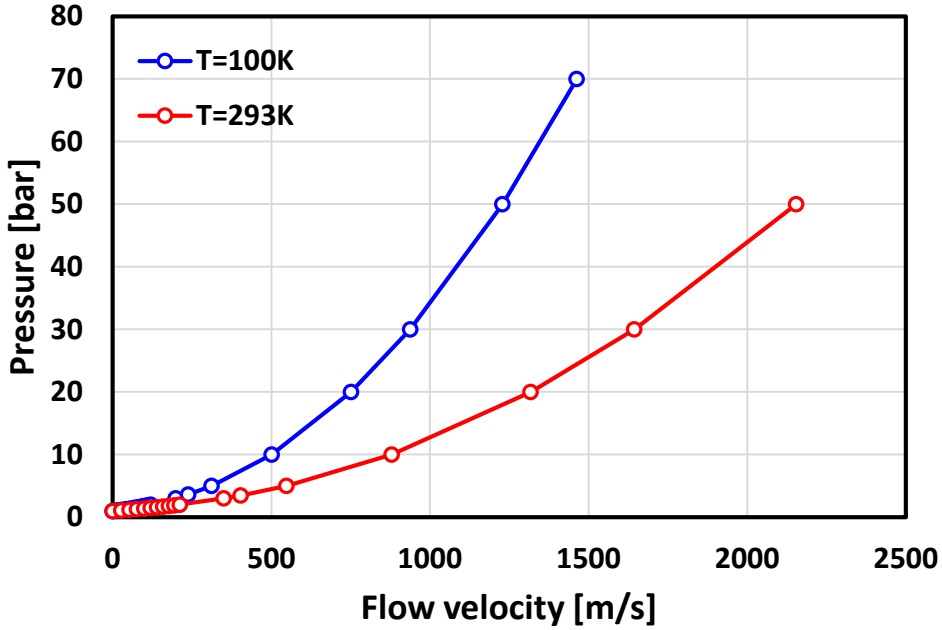

Figure 36. Dynamic pressure as a function of flow velocity calculated for stoichiometric hydrogen-air mixture at two temperatures.

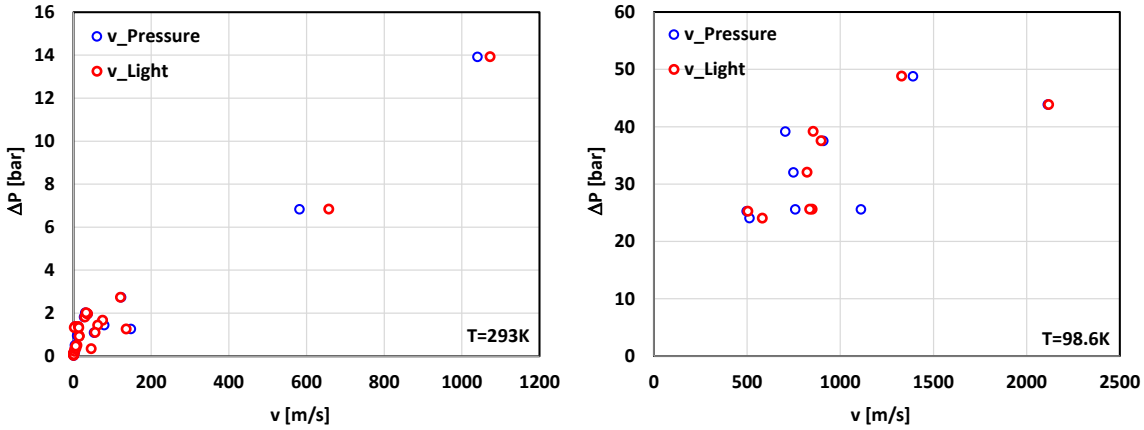

Figure 37. Maximum combustion pressure as function of characteristic flame velocity for the experiments in a smooth tube (BR=0%).

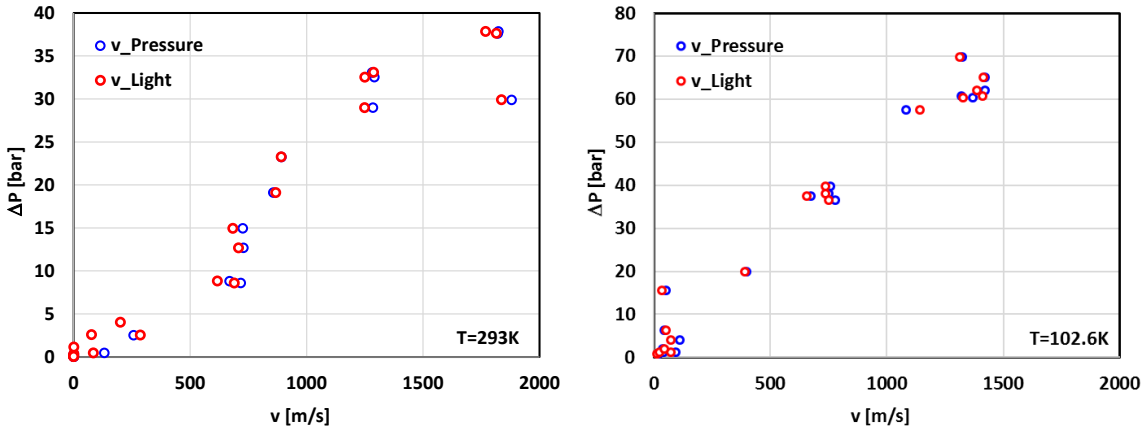

Figure 38. Maximum combustion pressure as function of characteristic flame velocity for the experiments in obstructed tube (BR=30%).

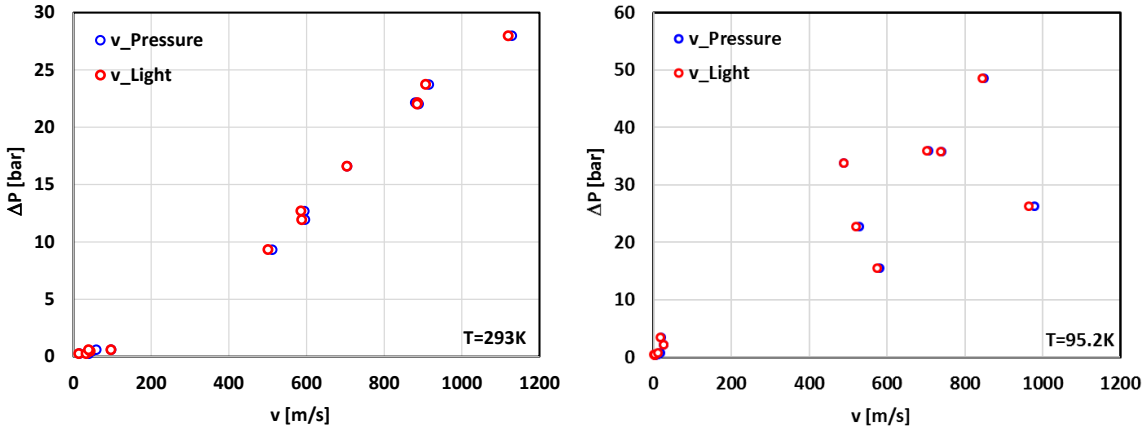

Figure 39. Maximum combustion pressure as function of characteristic flame velocity for the experiments in obstructed tube (BR=60%).

Adiabatic combustion pressure demonstrates the same difference of maximum combustion pressure for sonic deflagration and detonation regimes for all combustible mixtures Figure 40. The figure shows that even sonic deflagration produces the pressure 3 times higher than at ambient initial temperature and exceeds 1.5 times the detonation pressure at the ambient initial temperature. This means that cryogenic hydrogen combustion is much more dangerous than detonation at ambient temperature. To prevent such a development of the

combustion process the flame velocity shouldn't exceed the speed of sound in reactants (M <1). As we found, the criterion for such a scenario is the critical expansion ratio shouldn't be exceeded by the value for the tested combustible mixture $\sigma < \sigma^* = 12.5$. Figure 41 summarizes all experimental data of current work with an extension for elevated temperature T = 650 K from paper [2]. So that it covers the temperature range from cryogenic T = 90 K to elevated temperature T = 650 K. Open points show current experimental data on expansion ratios at different temperatures. With a good accuracy the boarding line between slow (M<1) and fast sonic deflagration (M>1) can be approximated by exponential dependence on initial temperature T[K]:

$$\sigma^* = 2200 \cdot T^{-1.12} \quad (4)$$

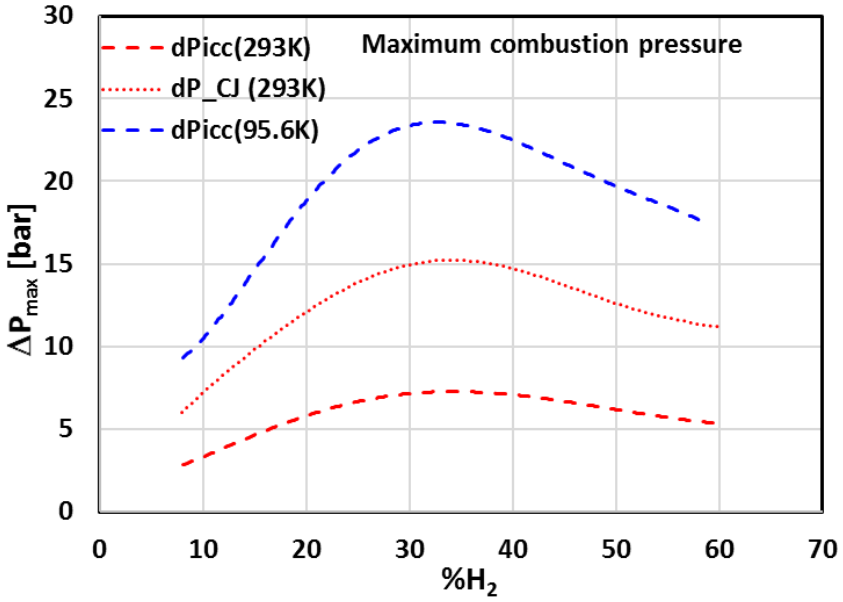

Figure 40. Theoretical maximum combustion pressure as function of hydrogen concentration at different initial temperatures.

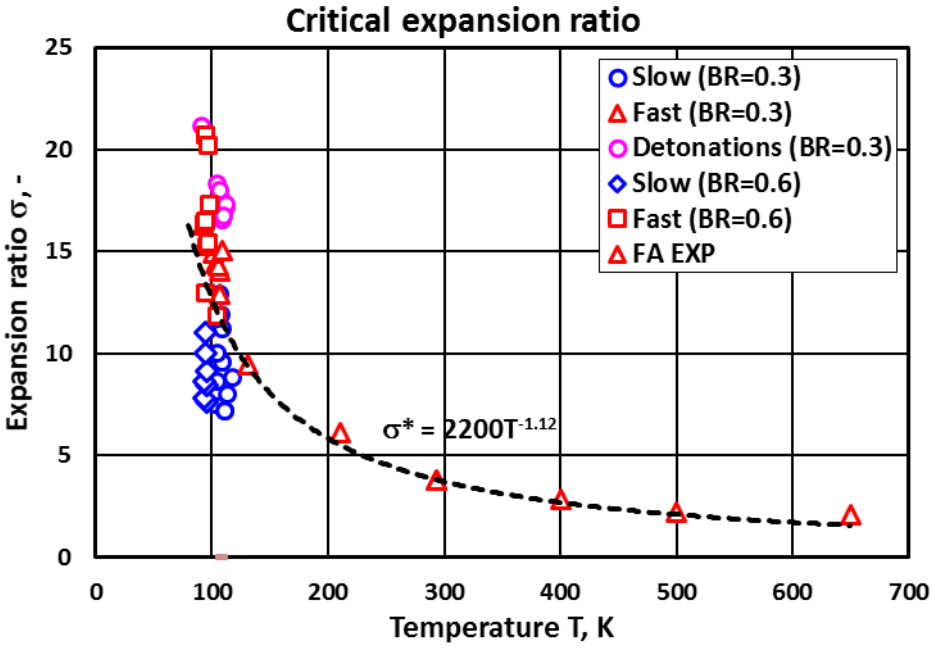

Figure 41. Critical expansion ratio as function of initial temperature based on experiments in obstructed tubes (BR=30% and BR = 60%).

The cut-off line for fast and slow deflagration described by equation Eq. (4) is very close to hyperbolic dependence on initial temperature. We may transform it as follows

$$\sigma^*(T) = \sigma^*(T_0)\cdot\left(\frac{T_0}{T}\right), \qquad (5)$$

where $\sigma^*(T_0) = 3.75$ at the ambient temperature $T_0 = 293$ K. Then, for T = 100 K we get more conservative values of $\sigma^*(T) = 11.0$ instead of $\sigma^*(T) = 12.6$ according to Eq. (5). But still, the Eq. (5) is very valuable for the prediction of flame acceleration limits at different temperatures.

Table 22: Main thermodynamic and combustion properties of tested mixtures at cryogenic temperature T = 100 K.

%H_2	To, K	Speed of sound		Adiabatic		Exp. ratio	Detonation		
		react.	prod.	temp.	press.		Press.	Veloc.	cell size
		c_r, m/s	c_p, m/s	T_b, K	ΔP_b, bar	σ	ΔP_{CJ}, bar	D_{CJ}, m/s	λ, mm
8	100	185	554	761	8.44	7.30	17.5	1141	
9	100	186	582	840	9.34	8.03	19.3	1200	
10	100	187	608	919	10.21	8.73	21.0	1256	
11	100	188	633	997	11.06	9.42	22.7	1309	
11	100	188	633	997	11.06	9.42	22.7	1309	
12	100	189	657	1074	11.88	10.10	24.4	1360	
15	100	193	723	1302	14.21	12.04	29.0	1499	λ > 170
16	100	194	744	1376	14.94	12.66	30.5	1542	λ > 170
17	100	195	764	1451	15.65	13.27	31.9	1583	λ > 170
18	100	196	784	1524	16.34	13.87	33.3	1623	λ = 170
19	100	197	803	1597	17.01	14.45	34.7	1662	λ<170
20	100	198	821	1669	17.66	15.02	36.0	1700	45<λ<170
22	100	201	857	1812	18.89	16.13	38.4	1772	45<λ<170
25	100	204	906	2017	20.57	17.67	41.8	1873	λ = 45.2
28	100	208	946	2205	21.99	19.02	44.7	1962	9.5<λ<45.2
29	100	210	956	2255	22.34	19.38	45.4	1987	9.5<λ<45.2
30	100	211	966	2284	22.56	19.59	45.8	2009	9.5<λ<45.2.2
34	100	217	997	2224	22.39	19.18	45.5	2064	9.5<λ<45.22
39	100	225	1014	2092	21.47	18.25	43.7	2104	9.5<λ<45.2.2
44	100	234	1029	1951	20.37	17.22	41.4	2137	9.5<λ<45.2
45	100	236	1032	1923	20.14	17.01	41.0	2144	9.5<λ<54
50	100	246	1046	1777	18.91	15.90	38.5	2174	10<λ<170
51	100	248	1048	1747	18.65	15.67	37.9	2179	10<λ<170
54	100	255	1056	1657	17.85	14.97	36.3	2196	
58	100	266	1066	1535	16.73	13.99	34.1	2218	
60	100	271	1070	1472	16.15	13.49	32.9	2228	

The next limit we found in current work at cryogenic temperatures is the detonability limit based on detonation cell sizes. Since we did not directly measure the detonation cell sizes at cryogenic temperatures, we used existing detonability limits for detonation cell size evaluation:

$$d > \lambda/\pi \text{ for detonation propagation in a smooth tube (BR = 0),} \qquad (6)$$

$$X_D < 500\cdot\lambda \text{ for run-up-distance in a smooth tube (BR = 0),} \qquad (7)$$

$d > \lambda$ for detonation propagation in an obstructed tube (BR = 30%), (8)

$d > 3 \cdot \lambda$ for detonation propagation in an obstructed tube (BR = 60%), (9)

where d is the characteristic diameter of the system: d = D a tube diameter for smooth tube; d = d an orifice size for the obstructed tube with BR = 30% and BR = 60%; X_D is the run-up-distance to detonation in a smooth tube. The most crucial limitation is given by Eq. (6) as $\lambda < 170$ mm, as the maximum detonation cell size for detonable mixtures in a tube of 54 mm diameter. This means that the mixtures with $\lambda > 170$ mm cannot detonate in our tube at all. All the criteria for detonation onset have been checked at ambient temperature with known detonation cell sizes. Then the criteria were extrapolated to cryogenic temperatures. The limitations for the detonability at cryogenic temperatures are separately given in Table 15 for BR=0%, in Table 18 for BR=30% and Table 21 for BR=60%. All the limitations from those tables are collected in Table 22 and shown in Figure 42. The figure shows some difference in detonation cell sizes at cryogenic and ambient temperature but much less than expected in our report D5.1. The data for detonation cell sizes at cryogenic temperature T=100K can be approximated as polynomial dependence on hydrogen concentration:

$$\lambda = 0.0006724[H_2]^4 - 0.1039[H_2]^3 + 6.0786[H_2]^2 - 159.74[H_2] + 1603.3 \quad (10)$$

where $[H_2]$ is the hydrogen concentration in volumetric percent.

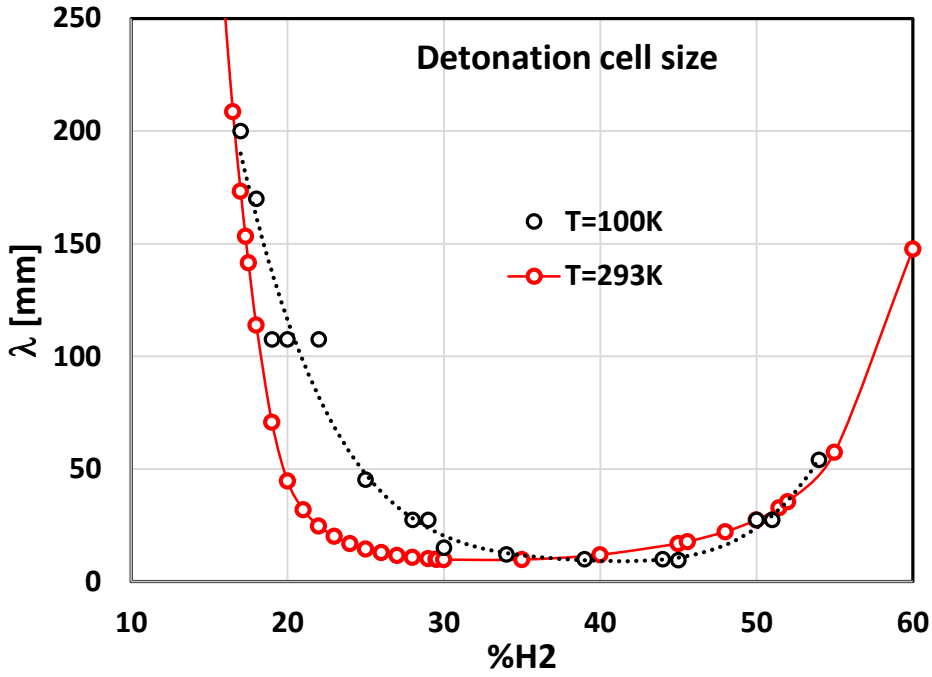

Figure 42. Experimental detonation cell size at cryogenic temperature T=100 K in comparison with the data at ambient temperature T = 293 K.

8 Data acquisition and data archiving.

Because the pressure and photo sensor recordings of some experiments contain more than 1 million samples, it is impossible to convert them to a spreadsheet file (".XLSX"). It was decided not to downsample them, to make them digestible by spreadsheet programs. Instead, the original recording in a ".TPC" file was converted to a CSV format file with extension ".ASC".

The structure of these files is simple. They are columnar comma separated tables. The first line contains the names of the channel and the second line contains the unit descriptions, see Figure 43(a). Original data for pressure sensors in Volts are converted to bar according to Table 23. The third line shows the start time of each channel (Figure 43(b)). Because of the simultaneous data acquisition, the start times are identical for all channels and can be omitted. The "Time" column gives the time relative to the trigger event. The trigger event is recorded in the "TRG" column. In fact, it should be synchronized with a spark plug but actually, it can be a delay between the trigger signal and spark actuation. Even, it might be no ignition phenomena.

Table 23: Conversion factors for pressure sensors (Volts to bar).

P01	6.3143
P02	11.1313
P03	6.6425
P04	10.9899
P05	6.7884
P06	11.2035
P07	6.2738
P08	11.1162
P09	6.7188
P10	11.31
P11	6.2666
P12	11.4045
P13	6.8781

Time, TRG, P01, P02, P03, P04, P05, P06, P07, P08, P09, P10, P11, P12, P13, F01, F02, F03, F04, F05, F07, F08, F09, F10, F11, F12, F13, F14, F15

s, V, bar, bar, bar, bar, bar, bar, bar, bar, bar, bar, bar, bar, V, V, V, V, V, V, V, V, V, V, V, V, V

(a)

Start time, 2020-06-09 13:05:44, 2020-06-09 13:05:44, 2020-06-09 13:05:44, 2020-06-09 13:05:44, 2020-06-09 13:05:44, 2020-06-09 13:05:44,

(b)

-2.09e-01, -1.750004e-02, 6.31e-02, -1.11e-01, -1.57e-01, 1.71e-01, -2.54e-01, 2.31e-01, -1.80e-01, -7.64e-02,

(c)

Figure 43. The structure of data file: (a) header; (b) start time of each channel; (c) data.

All experimental conditions (blockage ratio (BR), initial temperature, hydrogen concentration) and main results for each experimental series are given in Table 4, Table 7, Table 10, Table 13, Table 16, Table 19 of the report. The data files are published as zipped ASCII files via the PRESLHY repository on KITopen service: https://www.bibliothek.kit.edu/cms/english/kitopen.php.

The naming convention of the corresponding 7zip-files largely follows the one provided in the Data Management Plan at ambient temperature reads as follows:

PT**0**-25.7z

with PT indicating the PRESHY tube, the index **0** means a smooth tube with blockage ratio BR = 0%, then the test number 25 should be addressed to Table 4 for the reading of experimental conditions.

For cryogenic temperatures, it reads as follows:

PT**30**C-25.7z

with the meaning the PRESLHY tube experiment number 25 in an obstructed tube with blockage ratio BR = 30% at cryogenic temperatures. The experimental conditions should be addressed to Table 16 and test number 25.

The original results are also presented in graphic form as so called distance – time diagrams. The diagram for each test reads as follows:

PT0-24-long-**RT**.wmf

With the same meaning as for the raw data file with an additional index "long" or "short" according to captured registration time and prefix **RT** means distance (radius) – time diagram. WMF means the Windows Meta File format. For some of experiments, the distance-time diagrams are already explained in the report D5.5. Let us consider one more example PT0-24-long-RT.wmf (Figure 44). It corresponds to the test PT0-24 for the smooth tube with blockage BR = 0% at ambient temperature. Table 4 gives the hydrogen concentration 15.2% and the main result is slow (subsonic) deflagration (S). The distance-time diagram (Figure 44) shows pressure - and photodiode signals - time histories (horizontal axis, t in seconds) placed vertically in accordance with the real position in a tube (vertical axis, X in m). In Figure 44, the pink line goes through the points corresponding to the flame arrival time based on photodiode signals (blue lines). The slope of the flame trajectory in X-t coordinates is the flame velocity U_f:

$$U_f = \frac{X_{i+1} - X_i}{t_{i+1} - t_i} \tag{11}$$

where $X_{i+1} - X_i$ is the distance between two sensors; $t_{i+1} - t_i$ is the arrival time difference for sensors numbered i+1 and i. The values of local velocity (in pink) are put in Figure 44 between each two photodiodes. Pressure signals (red and green lines) show an oscillating pressure corresponding to pressure wave movement back and forth reflecting from the flanges. Maximum pressures for each pressure sensor are given in Table 24.

Table 24: Maximum pressure for each pressure sensor.

#	P01	P02	P03	P04	P05	P06	P07	P08	P09	P10	P11	P12	P13
X [m]	0.175	0.175	0.525	0.525	1.525	1.525	2.525	2.525	3.525	3.525	4.925	4.925	5
P_{max}[bar]	0.093	0.423	0.316	0.121	0.315	0.168	0.466	0.578	0.596	0.724	0.609	0.730	0.568

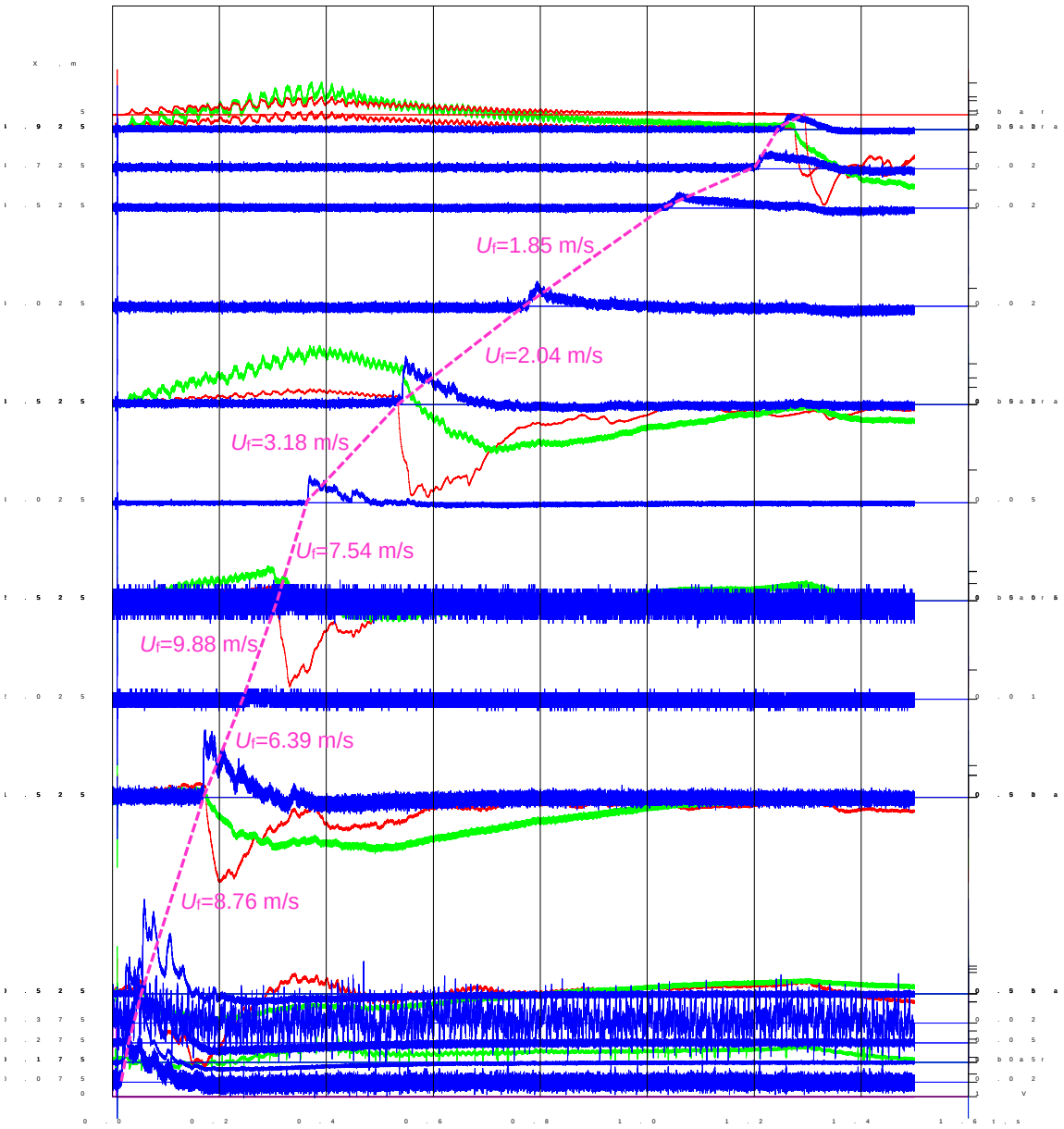

Figure 44. Distance-time diagram PT0-24-long-RT. wmf for the test PT0-24 (15.2% vol. H_2, BR=0%, T=293 K).

The right-hand side of the figure has signal scale in Volts for photodiodes or in bar for pressure sensors.

9 Summary, Conclusions and Outlook

In the frame of the PRESLHY project, more than 100 experiments were made with the Cryogenic Combustion Tube facility at HYKA KIT. About half of the experiments were made at cryogenic temperatures (approx. 80 to 130 K). During the experimental campaign, many difficulties were encountered as temperature nonuniformity, condensation of the mixture, ignition problems approaching the flammability limits, flame visualization and some others. It turned out to be impossible to ignite even hydrogen-rich mixtures at 77 K and it was not possible to achieve uniform temperatures along the tube at higher (approx. 150 K) temperatures. The photo sensors turned out to be too insensitive for slower

combustion processes with less intensive radiation. However, all the problems were satisfactory solved and the flame propagations regimes at cryogenic temperatures were found.

The critical conditions for flame acceleration were evaluated as a function of initial temperature within the range 90 – 650 K. It shows a much higher hydrogen concentration leading to sonic deflagration than was predicted by advanced extrapolation before the tests. The correlation based on current experiments is quite simple and useful:

$$\sigma^* = 2200 \cdot T^{-1.12} .$$

The run-up distance to sonic flame in a smooth tube at cryogenic temperature was found to be roughly two times shorter than at ambient temperature. For the first time a steady-state choking regime with the speed of sound in combustion products was registered in a smooth tube at cryogenic temperatures.

The detonation cell sizes at cryogenic temperature T = 100 K are evaluated on the basis of existing criteria for detonation onset in smoot and obstructed tubes and can be presented as a polynomial function of hydrogen concentration [H_2, % vol.]:

$$\lambda[\text{mm}] = 0.0006724[H_2]^4 - 0.1039[H_2]^3 + 6.0786[H_2]^2 - 159.74[H_2] + 1603.3.$$

With the measured detonation cell sizes, the well known detonability criteria can be used to assess the possibility of detonation for hydrogen –air mixtures at cryogenic temperatures in different geometries and scales.

It was experimentally found that the maximum combustion pressure at cryogenic temperatures is 2-3 times higher than that for ambient conditions. It demonstrates a high level of the danger under cryogenic hydrogen combustion. Theoretically, even adiabatic combustion pressure corresponding to sonic deflagration at cryogenic temperature is 1.5 times higher than the CJ-detonation pressure at ambient temperature.

All the data and criteria can be used for RCS recommendations and safety distance evaluations. Original experimental data will be valuable for numerical code validation as well.

10 References

1. Kuznetsov, M., Alekseev, V., Matsukov, I., Dorofeev, S. (2005) DDT in a smooth tube filled with a hydrogen–oxygen mixture. Shock Waves, 14: 205-215.

2. Dorofeev, S.B., Kuznetsov, M.S., Alekseev, V.I., Efimenko, A.A., Breitung, W. (2001) Evaluation of limits for effective flame acceleration in hydrogen mixtures. J. Loss Prev. Proc. Ind., 14 (6): 583-589.

3. Ciccarelli, G., Dorofeev, S. Flame acceleration and transition to detonation in ducts, Progress in Energy and Combustion Science, Volume 34, Issue 4, 2008, Pages 499-550

4. Dorofeev, S.B., Sidorov, V. P., Kuznetsov, M. S., Matsukov, I. D., Alekseev, V. I. (2000) Effect of scale on the onset of detonations. Shock Waves, v. 10, pp. 137-149.

5. Reynolds W.C., The Element Potential Method for Chemical Equilibrium Analysis: Implementation in the Interactive Program STANJAN Version 3, Dept. of Mechanical Engineering, Stanford University, Palo Alto, California, January 1986 (1986)

6. Gavrikov, A.I., A.A Efimenko, S.B Dorofeev (2000) A model for detonation cell size prediction from chemical kinetics, Combustion and Flame, 120 (1-2): 19-33

7. Teodorczyk A, Lee JH, Knystautas R (1988) Propagation mechanism of quasi-detonations. 22nd Symposium (Int.) on Combustion. The Combustion Institute, Pittsburgh, pp 1723–1731

8. Lee JH, Knystautas R, Chan CK (1984) Turbulent flame propagation in obstacle-filled tubes. 20th Symposium (Int.) on Combustion, The Combustion Institute, Pittsburgh, PA, pp 1663–1672

9. Kuznetsov M.S., Alekseev V. I., Dorofeev S. B. Comparison of critical conditions for DDT in regular and irregular cellular detonation systems. Shock Waves, 2000, v. 10, pp. 217-224

10. Ciccarelli, G., T. Ginsberg, J. Boccio, C. Economos, K. Sato, and M. Kinoshita. Detonation cell size measurements and predictions in hydrogen-air-steam mixtures at elevated temperatures. Combust. Flame, 99(2):212-220, 1994.

11. A. Veser, M. Kuznetsov, G. Fast, A. Friedrich, N. Kotchourko, G. Stern, M. Schwall, W. Breitung, The structure and flame propagation regimes in turbulent hydrogen jets, International Journal of Hydrogen Energy, Volume 36, Issue 3, 2011, Pages 2351-2359.